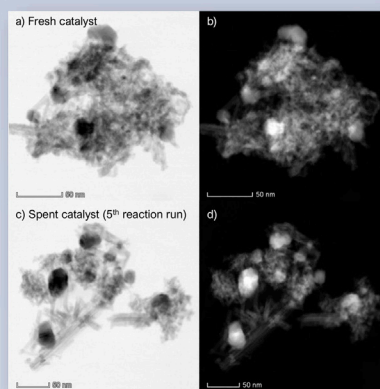
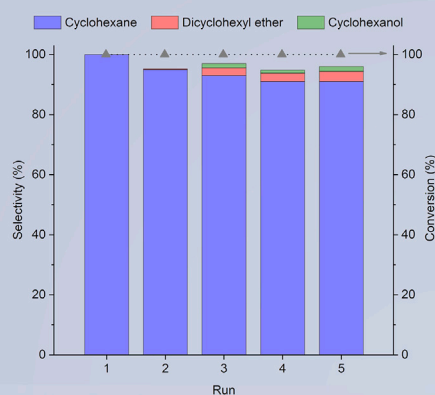


Article

Design of Nickel Supported on Water-Tolerant Nb₂O₅ Catalysts for the Hydrotreating of Lignin Streams Obtained from Lignin-First Biorefining

Understanding the Design of Catalysts for Lignin-to-Fuels



A key challenge in the design of solid catalysts for the HDO of lignin streams is identified:



Glauco F. Leal, Sérgio Lima, Inês Graça, ..., Antonio Aprigio S. Curvelo, Cristiane B. Rodella, Roberto Rinaldi

rrinaldi@ic.ac.uk

HIGHLIGHTS

Stable Ni/Nb₂O₅ catalyst for the hydrotreating of diphenyl ether produced

Key challenge in the design of solid catalysts for the HDO of lignin streams identified

Lewis acidity crucial to HDO also assists catalyst deactivation via coke formation

Recommendations for the catalyst design for lignin hydrotreating put forward

Leal et al., iScience 15, 467–488
 May 31, 2019 © 2019 The Author(s).
<https://doi.org/10.1016/j.isci.2019.05.007>

Article

Design of Nickel Supported on Water-Tolerant Nb₂O₅ Catalysts for the Hydrotreating of Lignin Streams Obtained from Lignin-First Biorefining

Glauco F. Leal,^{1,2,3} Sérgio Lima,¹ Inês Graça,¹ Heloíse Carrer,³ Dean H. Barrett,^{3,5} Erico Teixeira-Neto,⁴ Antonio Aprigio S. Curvelo,² Cristiane B. Rodella,³ and Roberto Rinaldi^{1,6,*}

SUMMARY

In biomass conversion, Nb₂O₅ has attracted increasing attention as a catalyst support presenting water-tolerant Lewis acid sites. Herein, we address the design of Ni/Nb₂O₅ catalysts for hydrotreating of lignin to hydrocarbons. To optimize the balance between acidic and hydrogenating properties, the catalysts were first evaluated in the hydrotreating of diphenyl ether. The best catalyst candidate was further explored in the conversion of lignin oil obtained by catalytic upstream biorefining of poplar. As primary products, cycloalkanes were obtained, demonstrating the potential of Ni/Nb₂O₅ catalysts for the lignin-to-fuels route. However, the Lewis acidity of Nb₂O₅ also catalyzes coke formation via lignin species condensation. Thereby, an acidity threshold should be found so that dehydration reactions essential to the hydrotreatment are not affected, but the condensation of lignin species prevented. This article provides a critical “beginning-to-end” analysis of aspects crucial to the catalyst design to produce lignin biofuels.

INTRODUCTION

Niobia (Nb₂O₅) has attracted a great deal of attention for catalytic applications in aqueous media owing to its water-tolerant Lewis acidity (Barrios et al., 2017; Brayner and Bozon-Verduraz, 2003; Chan et al., 2017; Chary et al., 2003; Francisco et al., 2004; Graça et al., 2013; Guan et al., 2017; Herval et al., 2015; Holtzberg et al., 1957; Jasik et al., 2005; Ko et al., 1984; Lopes et al., 2014; Nakajima et al., 2013; Rojas et al., 2013; Solcova et al., 1993; Tanabe and Okazaki, 1995; Valencia-Balvín et al., 2014; Wojcieszak et al., 2006). Generally, amorphous Nb₂O₅ shows high surface acidity, which is related to its high specific surface area and number of surface defects (do Prado and Oliveira, 2017; Ziolk and Sobczak, 2017). However, amorphous Nb₂O₅ is a fragile material, susceptible to changes by temperature and pressure (Pinto et al., 2017; Wojcieszak et al., 2006). Considering Nb₂O₅ crystalline phases, they are formed by distorted octahedra (NbO₆), connected by edges and corners. The distortion degree of NbO₆ octahedra depends on the polymorph structure (Nico et al., 2016; Pinto et al., 2017; Valencia-Balvín et al., 2014). This distortion leads to varied textural and structural stabilities as well as different surface acid properties and, therefore, impacts on catalytic properties. H-Nb₂O₅ (monoclinic structure) and T-Nb₂O₅ (orthorhombic structure) are the most common crystalline phases, whereas the TT-Nb₂O₅ (pseudo-hexagonal structure) is the least thermodynamically stable phase and is often considered as a less ordered form of the T-phase. By increasing the temperature and pressure in hydrothermal synthesis, the conversion of Nb₂O₅ phases takes place following the sequence: amorphous Nb₂O₅ → TT-Nb₂O₅ → T-Nb₂O₅ → H-Nb₂O₅ (Nowak and Ziolk, 1999; Pinto et al., 2017; Valencia-Balvín et al., 2014). Nb₂O₅ phase transitions are typically followed by a progressive decrease in the surface area, porosity, and acidity (Ali et al., 2017; Graça et al., 2013; Kreissl et al., 2017; Pinto et al., 2017; Raba et al., 2016; Valencia-Balvín et al., 2014). Among the crystalline phases, the TT-Nb₂O₅ phase is the one presenting the highest number of oxygen vacancies in the structure, and so the greatest degree of polyhedral distortion (Pinto et al., 2017; Rani et al., 2014). TT-Nb₂O₅ is characterized by the presence of distorted octahedra and pentagonal and hexagonal bipyramids, i.e., NbO₆, NbO₇, and NbO₈ polyhedra, which are the structural units also present in amorphous Nb₂O₅ (Nakajima et al., 2011; Nico et al., 2016). Notably, TT-Nb₂O₅ structural features translate into a highly polarized and disordered surface with high levels of Lewis and Brønsted acid sites, which are essential to the high performance of hydrodeoxygenation (HDO) catalysts.

Metal-based (mainly Pt, Pd, Ru, Ni) catalysts supported on acidic materials have been widely examined in the HDO of lignin model compounds (Cui et al., 2017; Shao et al., 2017; Teles et al., 2018; Wang and Rinaldi,

¹Department of Chemical Engineering, Imperial College London, South Kensington Campus, London SW7 2AZ, UK

²Department of Physical Chemistry, Institute of Chemistry of São Carlos, University of São Paulo, Av. Trabalhador São Carlense, 400, São Carlos, São Paulo 13566-590, Brazil

³Brazilian Synchrotron Light Laboratory (LNLS), Brazilian Center for Research in Energy and Materials (CNPEM), Campinas, São Paulo 13083-970, Brazil

⁴Brazilian Nanotechnology National Laboratory (LNNano), Brazilian Center for Research in Energy and Materials (CNPEM), Campinas, São Paulo 13083-970, Brazil

⁵School of Chemistry, University of the Witwatersrand, Johannesburg, South Africa

⁶Lead Contact

*Correspondence: rrinaldi@ic.ac.uk

<https://doi.org/10.1016/j.isci.2019.05.007>



2016; Zhao et al., 2009). For the HDO of lignin model compounds and lignin streams, niobium oxides have been studied as supports for noble metals (Shao et al., 2017). Studies on multifunctional $\text{Fe}_3\text{O}_4/\text{Nb}_2\text{O}_5/\text{Co}/\text{Re}$ catalysts have also been reported (Parvulescu et al., 2017). Pd catalysts supported on niobia revealed promising results for the dehydroxylation of phenol to benzene, presenting a reaction rate 90-fold higher than that observed for a Pd/ SiO_2 catalyst (Barrios et al., 2017). Importantly, Pt/ $\text{Nb}_2\text{O}_5\text{-Al}_2\text{O}_3$ has been reported as an active catalyst for the hydrotreating of diphenyl ether, showing stability higher than that of Pt/ Al_2O_3 owing to the water-tolerant nature of niobium(V) Lewis acid sites (Jeon et al., 2018). Subjecting lignin-derived dimers to a $\text{Ni}_{0.92}\text{Nb}_{0.08}$ catalyst resulted in full conversion of the substrates into liquid alkanes at 200°C after 2 h, demonstrating the outstanding ability of this material for C–O cleavage and HDO (Jin et al., 2017). For the selective production of arenes from lignin, it was reported that Ru- Nb_2O_5 catalysts present unique catalytic properties, compared with Ru supported on traditional oxide supports (Shao et al., 2017).

In an approach for lignin-to-liquid fuels, one of the challenges is to design inexpensive catalysts with high activity, selectivity, and stability under process conditions. Since the hydrotreating of lignin streams releases water, the solid catalyst must be stable in the presence of water under high-severity conditions. Commercial niobia ($\text{Nb}_2\text{O}_5 \cdot x\text{H}_2\text{O}$) is a bulk amorphous material that lacks stability under hydrothermal conditions, thus losing surface area and leading to the sintering of supported metallic particles (Pham et al., 2011). To overcome the poor structural stability of commercial Nb_2O_5 , various synthesis methods have been a subject of research in producing highly stable nanostructured materials (Zhao et al., 2012b). Nb_2O_5 nanoparticles with no defined shape can be obtained by precipitation and sol-gel synthesis methods followed by calcination. These routes have extensively been studied in the preparation of the Nb_2O_5 supports applied to the HDO of lignin and lignin-derived molecules with good results (Shao et al., 2017). Nb_2O_5 crystallization under low-severity solvothermal conditions constitutes another progress in this field. This synthetic route produces single TT- Nb_2O_5 nanorods with controlled size and morphology, high surface area, and improved acid properties (Ali et al., 2017; Leite et al., 2006; Zhou et al., 2008). TT- Nb_2O_5 nanorods exhibit shape-dependent acidic sites (Zhao et al., 2012a). On (001) TT- Nb_2O_5 surface of the nanorods, Lewis acid sites are much stronger than those of spherical Nb_2O_5 particles. Despite the interesting acidic properties, the production of Nb_2O_5 nanorods employs oleic acid and trioctylamine as structure-directing agents in the solvothermal synthesis. Especially for catalytic applications, the use of such structure-directing agents surfactants in the synthesis of Nb_2O_5 presents disadvantages owing to their high costs, low volume of material production limitation, and the need to remove the agents via calcination, which may modify the morphology, particle size, and surface chemistry of Nb_2O_5 (Ali et al., 2017; Zhao et al., 2012a).

Hydrothermal synthesis of TT- Nb_2O_5 nanorods in the presence of H_2O_2 represents a route receiving far less attention, but with the most promising results regarding the textural and acidic properties of niobia (Leal et al., 2019). Despite the improved chemical and physical properties, such Nb_2O_5 nanorods have not yet been explored in the chemistry of lignin hydrotreating. Therefore, this knowledge gap brought us to the study of nickel supported on hydrothermally stable TT- Nb_2O_5 nanorods as a potential catalyst for HDO of lignin streams. As about 80% of the primary interunit linkages of lignin are ether bonds (Rinaldi et al., 2016), and a considerable number of other oxygenated functionalities are present in lignin-derived phenolics, a highly stable and highly acidic niobia could well hold the key to produce efficient catalysts for lignin-to-liquid fuels, owing to an expected synergism between metal phase and support toward lignin depolymerization and acid-catalyzed deoxygenation of intermediates formed throughout the HDO course (Cao et al., 2018; Wang and Rinaldi, 2016, 2013).

In this report, we examine the catalytic properties of Ni-supported on TT- Nb_2O_5 nanorods for the hydrotreating of a model compound (diphenyl ether) and lignin oil produced by a lignin-first biorefining process based on H-transfer reductive processes, the so-called catalytic upstream biorefining (CUB), which is also denoted as ‘*reductive catalytic fractionation*’ (RCF) by several research groups. CUB constitutes a class of methods for deconstruction of lignocellulose that renders high-quality pulps together with depolymerized and passivated lignin streams (Ferrini and Rinaldi, 2014; Galkin and Samec, 2016; Graça et al., 2018; Rinders et al., 2017; Rinaldi, 2017; Schutyser et al., 2018; Sultan et al., 2019; Rinaldi et al., 2019). TT- Nb_2O_5 nanorods were prepared via hydrothermal synthesis by employing ammonium niobium oxalate and H_2O_2 as the structure-directing agent (Leal et al., 2019; Leite et al., 2006; Pavia et al., 2010). TT- Nb_2O_5 nanorods were then loaded with several Ni contents. In this report, the results and discussion are organized as follows. First, the characterizations of the as-synthesized TT- Nb_2O_5 nanorods and Ni/ Nb_2O_5 catalysts are

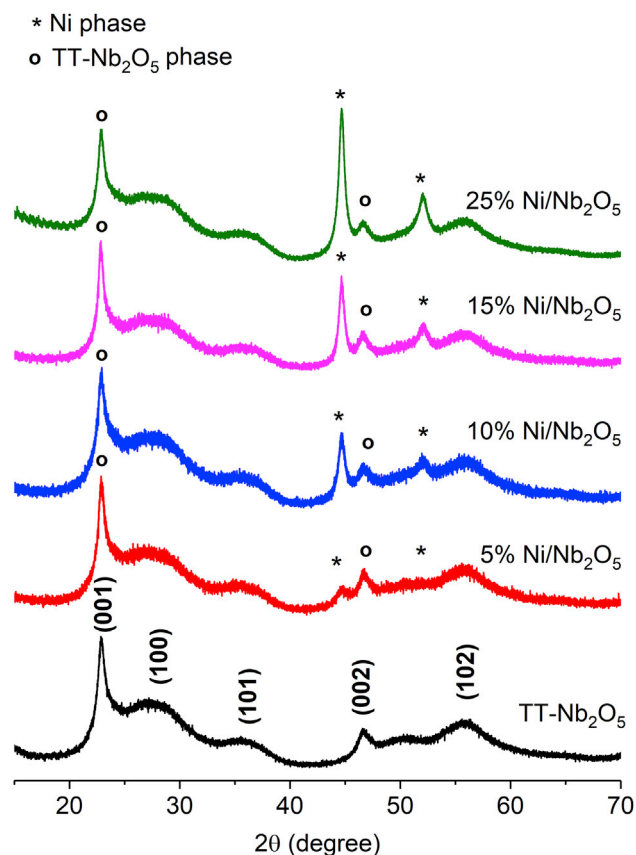


Figure 1. XRD Patterns of TT-Nb₂O₅ and Reduced Ni/Nb₂O₅ Catalysts

The asterisks indicate Ni(111) and Ni(200) reflections at 44.6° and 52.1°, respectively.

briefly presented. Ni/Nb₂O₅ catalysts are subsequently applied to the HDO of diphenyl ether at 160°C and 200°C under 4 MPa H₂. The catalyst performance and stability in the HDO of diphenyl ether at 200°C under 4 MPa H₂ were assessed. Finally, under more severe conditions (300°C and 7 MPa H₂), the 15%Ni/Nb₂O₅ catalyst was applied to the hydrotreating of the lignin oil.

RESULTS AND DISCUSSION

Characterizations of Ni/Nb₂O₅ Catalysts

Figure 1 shows the X-ray diffraction (XRD) patterns obtained from both the hydrothermally as-synthesized Nb₂O₅ after calcination at 380°C and Ni/Nb₂O₅ catalysts reduced at 320°C. XRD pattern of the Nb₂O₅ support exhibits peaks characteristic of the pseudo-hexagonal TT-Nb₂O₅ phase (Ko and Weissman, 1990). Notably, a high-intensity signal is observed at 22.8°, which is associated with (001) reflection of TT-Nb₂O₅. In addition, a low-intensity and broad signal related to the (100) plane appears at 28.0°. As next confirmed by scanning transmission electron microscopic (STEM) imaging, a preferred growth of TT-Nb₂O₅ along the (001) direction creates the preferential orientation feature in the XRD pattern, indicating the formation of TT-Nb₂O₅ as nanorods (Ali et al., 2017). For the Ni/Nb₂O₅ materials, the XRD patterns demonstrated that the structural features of the TT-Nb₂O₅ phase were preserved after the reduction procedure. Hence, for simplicity, when referring to the materials produced in this study, the TT-Nb₂O₅ phase will be denoted as “Nb₂O₅” henceforth. As expected, Ni(111) and Ni(200) reflections are observed at 44.6° and 52.1°. These reflections become more intense and sharper with an increase in Ni content from 5 to 25 wt %. Considering the Ni(111) reflection, the average Ni crystallite sizes estimated by the Scherrer equation grow from 7 to 15 nm with the rise in Ni content from 5 to 25 wt % (Table 1).

To verify whether the synthesis rendered Nb₂O₅ nanorods, the Nb₂O₅ material was examined by using high-angle annular dark-field (HAADF)-STEM (Figure 2). The HAADF-STEM images show that the

Sample	Actual Ni Content (%) ^a	Average Ni Crystallite Size (nm) ^b	BET Surface Area (m ² g ⁻¹) ^c
Nb ₂ O ₅	–	–	196
5%Ni/Nb ₂ O ₅	4.8	7	219
10%Ni/Nb ₂ O ₅	9.4	12	181
15%Ni/Nb ₂ O ₅	13.9	14	180
25%Ni/Nb ₂ O ₅	23.8	15	141

Table 1. Ni Content, Ni Crystallite Size, and Textural Properties of Nb₂O₅ and Ni/Nb₂O₅ Materials

^aDetermined by inductively coupled plasma mass spectrometry (ICP-MS) analysis.

^bEstimated by XRD by applying the Scherrer equation to the reflection of Ni(111) at 44.6°.

^cDetermined by N₂ physisorption measurements at –196°C.

hydrothermal synthesis produced Nb₂O₅ nanorods with approximately 8–25 nm length and 3–4 nm width (Leal et al., 2019). The nanorod dimensions are in line with those of previous studies showing that the crystal growth in the hydrothermal method follows an oriented attachment mechanism (Leite et al., 2006), producing nanorods smaller than those synthesized in the presence of a surfactant as a shape-directing agent. In fact, surfactant-based syntheses yield large particles, owing to a decrease in the rate of crystal growth (Zhao et al., 2012a). In turn, longer (200–500 nm) and thinner (5–20 nm) TT-Nb₂O₂ nanorods were produced by a synthesis employing oleic acid as a structure-directing agent and ammonium niobium oxalate hydrate as the starting material (Zhao et al., 2012b).

Table 1 summarizes the textural properties of the support and Ni/Nb₂O₅ materials. N₂ adsorption-desorption isotherms are presented in Figure S1. Nb₂O₅ and Ni/Nb₂O₅ materials exhibit a type II isotherm with an H3 hysteresis (Thommes et al., 2015), corroborating the non-structural porosity created by the packing of Nb₂O₅ nanorods. Niobium oxide nanoparticles can be obtained by various synthesis methods, which leads to the preparation of materials of different shapes with Brunauer-Emmett-Teller (BET) specific surface areas that can range from about 20 m² g⁻¹ to 530 m² g⁻¹ (Luisa Marin et al., 2014; Morais et al., 2017; Shao et al., 2017). Table 1 shows the as-synthesized Nb₂O₅ support to possess a relatively high specific surface area (196 m² g⁻¹). Notably, no significant decrease in the surface area of Ni/Nb₂O₅ materials, with 5–15 wt % Ni loading on Nb₂O₅ was observed. Likewise, as the porosity of the Nb₂O₅ support is non-structural, the deposition of Ni phase onto the nest of nanorods does not significantly decrease the specific surface area. However, for 25%Ni/Nb₂O₅, the specific surface area slightly decreased (from 196 m² g⁻¹ to 141 m² g⁻¹).

Temperature-programmed reduction (TPR) profiles of the Nb₂O₅ nanorods and Ni/Nb₂O₅ precursors (catalysts before reduction) are shown in Figure 3. The TPR profiles of Ni/Nb₂O₅ precursors exhibit two reduction events. The first occurs at around 335°C. This event is assigned to the reduction of Ni(II) to Ni(0). The reduction temperature of the Ni(II) species supported on Nb₂O₅ nanorods is much lower than that of bulk NiO (450°C) (Graça et al., 2014). Nevertheless, the range of Ni reduction temperatures between 320°C and 345°C is in line with previous studies on Ni/Nb₂O₅ materials containing high nickel loadings (Janković et al., 2008; Liu et al., 2016). Interestingly, and contrary to what has been previously observed by other research groups (Chary et al., 2003; Wojcieszak et al., 2006), no shift of the Ni reduction peak to higher temperatures with an increase in Ni loading was observed. As will be presented later, in the 15%Ni/Nb₂O₅ material, the Ni nanoparticles are embedded in a nest formed by Nb₂O₅ nanorods (Figure 11). Thereby, such an entanglement of metal phase and oxidic support may result in few (but strong) connecting points between these phases so that an effect of the increase in the Ni loading on the reduction temperature of NiO species is not apparently observed. However, in the second reduction (at about 800°C), which is related to the partial reduction of Nb₂O₅ to NbO₂ (Wojcieszak et al., 2006), the temperature required for the reduction of Nb₂O₅ progressively decreases (from 870°C to 816°C) with increasing Ni content (Table S1). This observation indicates that there is an interaction between Ni and NbO₅ phases in which the hydrogen spillover appears to be more prevalent for the samples containing higher Ni loadings.

Nb₂O₅ polymorph crystals are formed by distorted octahedra (NbO₆) connected by edges and corners, the degree of distortion depending on the polymorph structure (Nico et al., 2016; Pinto et al., 2017; Valencia-Balvín et al., 2014). In the TT-Nb₂O phase, the highly distorted octahedra (NbO₆) units exhibit Nb=O

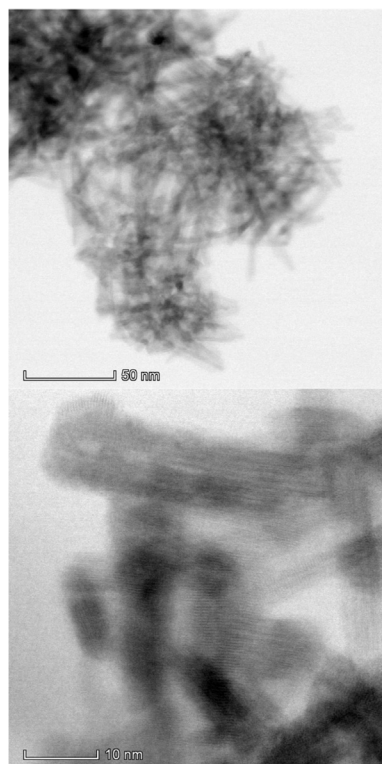


Figure 2. HAADF-STEM Images of TT-Nb₂O₅ Nanorods

bonds, enabling the Nb(V) center to act as a Lewis acid site. In turn, the slightly distorted NbO₆, as well as NbO₇ and NbO₈ groups, only present Nb-O bonds, which provide scaffolding for the [Nb(V)—OH₂²⁺] Brønsted acid sites (Chan et al., 2017). In this study, we found the quantity of Lewis acid sites on Nb₂O₅ (210 μmol g⁻¹) to be higher than that of Brønsted acid sites (143 μmol g⁻¹, Figure S2 and Table S2).

To assess the nature of the acidic sites of Nb₂O₅ support and Ni/Nb₂O₅ catalysts (after the reduction procedure), attenuated total reflection (ATR)-Fourier transform infrared (FTIR) spectra of adsorbed pyridine (Py) were collected (Figure 4). We chose to assess the nature of acid sites by ATR technique because of the dark color of the activated Ni/Nb₂O₅, which hinders FTIR transmission experiments (as those performed on the Nb₂O₅ support). Pyridine adsorbed on the materials exhibits infrared (IR) bands at around 1,446 cm⁻¹ and 1,606 cm⁻¹. These bands are related to the Py coordinated to Lewis acid sites. In addition, the IR spectra show bands at 1,639 cm⁻¹ and 1,540 cm⁻¹, which are assigned to the formation of the pyridinium ion (PyH⁺) on Brønsted acid sites (Figure 4) (Datka, 1992; Dollish et al., 1974; Iizuka et al., 1983; Parry, 1963). An IR band of adsorbed Py common to both Lewis and Brønsted acid sites is also visible at 1,489 cm⁻¹. These observations indicate that both Lewis and Brønsted acid sites are present in the Nb₂O₅ nanorods. From the relative intensities of Py adsorbed on Lewis and Brønsted acid sites, it can be inferred that the Brønsted acidity decreases as the Ni loading increases, as indicated by the reduction in the intensities of the bands at 1,639 cm⁻¹ and 1,540 cm⁻¹. This finding is explained by the ion exchange of Brønsted acid sites by the positively charged Ni species. However, in the 25%Ni/Nb₂O₅ catalyst, the support still presents some residual Brønsted acidity. Notably, the Lewis acidity (bands at around 1,606 cm⁻¹ and 1,446 cm⁻¹) appears to be mostly preserved even at such a high loading of Ni on Nb₂O₅ nanorods.

Acid supports are active in the dehydration of cyclohexanol to cyclohexene and, therefore, are vital to the hydrotreating of lignin to alkanes and arenes (Wang and Rinaldi, 2016; Zhao et al., 2010, 2009). Hence, to further assess the effect of Ni loading on the acidic properties of the catalysts, cyclohexanol dehydration was carried out at 200°C. As will be presented in the next section, this reaction is key to produce

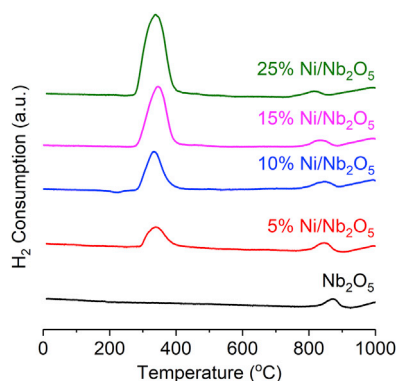


Figure 3. H₂-TPR Profiles for Nb₂O₅ Support and Ni/Nb₂O₅ Catalyst Precursors

cyclohexane from the conversion of diphenyl ether, as well as to obtain cycloalkanes from lignin. Table 2 summarizes the cyclohexanol conversion values obtained after 30 min of reaction at 200°C.

As expected, for the Nb₂O₅ nanorods, cyclohexanol conversion is considerably high. However, cyclohexanol conversion significantly decreases in the presence of 5%Ni/Nb₂O₅ catalyst. By increasing Ni loadings, cyclohexanol conversion continually drops, plateauing at 31% for 25%Ni/Nb₂O₅. These results show that the activity of the catalysts is partially affected by Ni deposition. Overall, the results presented in Table 2 indicate that the decrease in Brønsted acidity is detrimental to the dehydration performance. These results confirm that, at promoting the dehydration of cyclohexanol, Brønsted acid sites are more active for alcohol dehydration than the Lewis acid sites (Foo et al., 2014).

Hydrodeoxygenation of Diphenyl Ether

The catalytic performance of the Ni/Nb₂O₅ catalysts was evaluated for the conversion of diphenyl ether as a model reaction. The cleavage of diphenyl ether serves as a model reaction for the breakdown of 4-O-5 ether linkages occurring in lignins. Owing to its high bond dissociation enthalpy (BDE: 330 kJ mol⁻¹), the 4-O-5 linkages are resistant against cleavage via non-catalytic thermal processes, compared with α-O-4 and β-O-4 ether linkages occurring both in native and technical lignins (BDE: 215 kJ mol⁻¹ for α-O-4 in phenylcoumaran subunits, and 290–305 kJ mol⁻¹ for β-O-4 in lignin's aryl alkyl ether-bonding motifs) (Dorrestijn et al., 2000; Parthasarathi et al., 2011; Rinaldi et al., 2016; Wang and Rinaldi, 2012; Younker et al., 2011). Therefore, the ability of a Ni catalyst for hydrogenolysis can be evaluated with little contribution of thermolysis to the overall reaction results. In this instance, diphenyl ether is also a useful model compound for another reason. It allows for the evaluation of the activity of the Ni phase toward hydrogenation of phenol and benzene, the intermediates formed by the hydrogenolysis of diphenyl ether. In the presence of acid sites, the intermediate mixture is ultimately funneled to cyclohexane, as schematically represented by the reaction network presented in Figure 5.

To investigate the different catalyst functionalities, the hydrotreating of diphenyl ether was carried out at two temperatures, 160°C and 200°C. These two conditions were chosen because dehydration of alcohols has significant enthalpic barriers for the formation of carbocations (Liu et al., 2017), meaning that relatively high temperatures are required for the alcohol dehydration. By this choice, the hydrogenolysis and hydrogenation extents can be better discerned in the experiments carried out at 160°C, whereas the performance for the full HDO of diphenyl ether is better addressed by the experiments performed at 200°C.

When targeting cycloalkanes, the results of a model compound reaction can be more conveniently compared by computing the HDO extent and degree of deoxygenation (DOD), as given by Equations 1 and 2, respectively (Rinaldi, 2015).

$$\text{HDO extent} = \frac{H_2 \text{ incorporated in the products}}{H_2 \text{ for complete conversion to cyclohexane}} \times 100 \quad (\text{Equation 1})$$

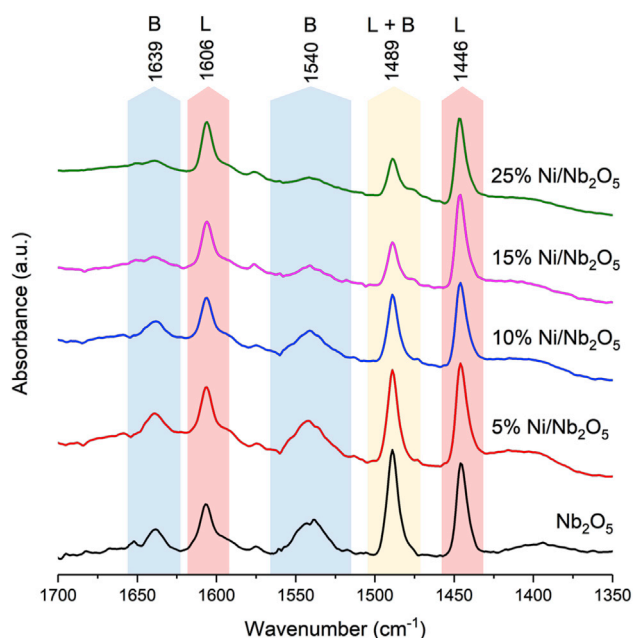


Figure 4. ATR-FTIR Spectra of Adsorbed Pyridine on Nb_2O_5 and Reduced $\text{Ni}/\text{Nb}_2\text{O}_5$ Catalysts

$$\text{DOD} = \left(1 - \frac{\text{wt \% O in product}}{\text{wt \% O in feed}} \right) \times 100 \quad (\text{Equation 2})$$

Figure 6A compares the performance of the $\text{Ni}/\text{Nb}_2\text{O}_5$ by evaluating the HDO extent achieved by the reaction network as a function of time for the conversion of diphenyl ether at 160°C . As expected, an increase in HDO extent with time for all tested catalysts was observed. By analyzing the results obtained at 180 min (Figure 6B), the HDO extent increased linearly from 28% to 46% with the rise in the Ni content (from 5 to 25 wt %). On the other hand, as expected at this temperature, low DOD was obtained for all catalysts at 180 min, with a decrease being in general noticed with the increase in Ni content, owing to the decline in the Brønsted acidity, as previously discussed. In these experiments, conversions of diphenyl ether in the range of 55%–98% at 180 min were achieved (Figure 6B). A blank test and a catalytic run with the pure Nb_2O_5 were also carried out (Table S3). By stark contrast, in these control experiments, only very low conversion of diphenyl ether (8% and 15%, respectively) was achieved at 180 min, with no selectivity to a specific product. Furthermore, to verify whether there is a contribution of the leached species to the reactions, the catalyst 15% $\text{Ni}/\text{Nb}_2\text{O}_5$ was contacted with the solvent under the same conditions of the reaction. After this, the catalyst was separated from the liquid product, and then diphenyl ether and the internal standard were added to the reaction media for reaction run. The results were similar to those of the blank reaction, confirming that the catalytic process is exclusively taking place on the catalyst surface.

Catalyst	Cyclohexanol Conversion (%)
No added catalyst	3
Nb_2O_5	75
5% $\text{Ni}/\text{Nb}_2\text{O}_5$	40
10% $\text{Ni}/\text{Nb}_2\text{O}_5$	37
15% $\text{Ni}/\text{Nb}_2\text{O}_5$	31
25% $\text{Ni}/\text{Nb}_2\text{O}_5$	31

Table 2. Cyclohexanol Conversion as a Function of Ni Amount Deposited on Nb_2O_5 .

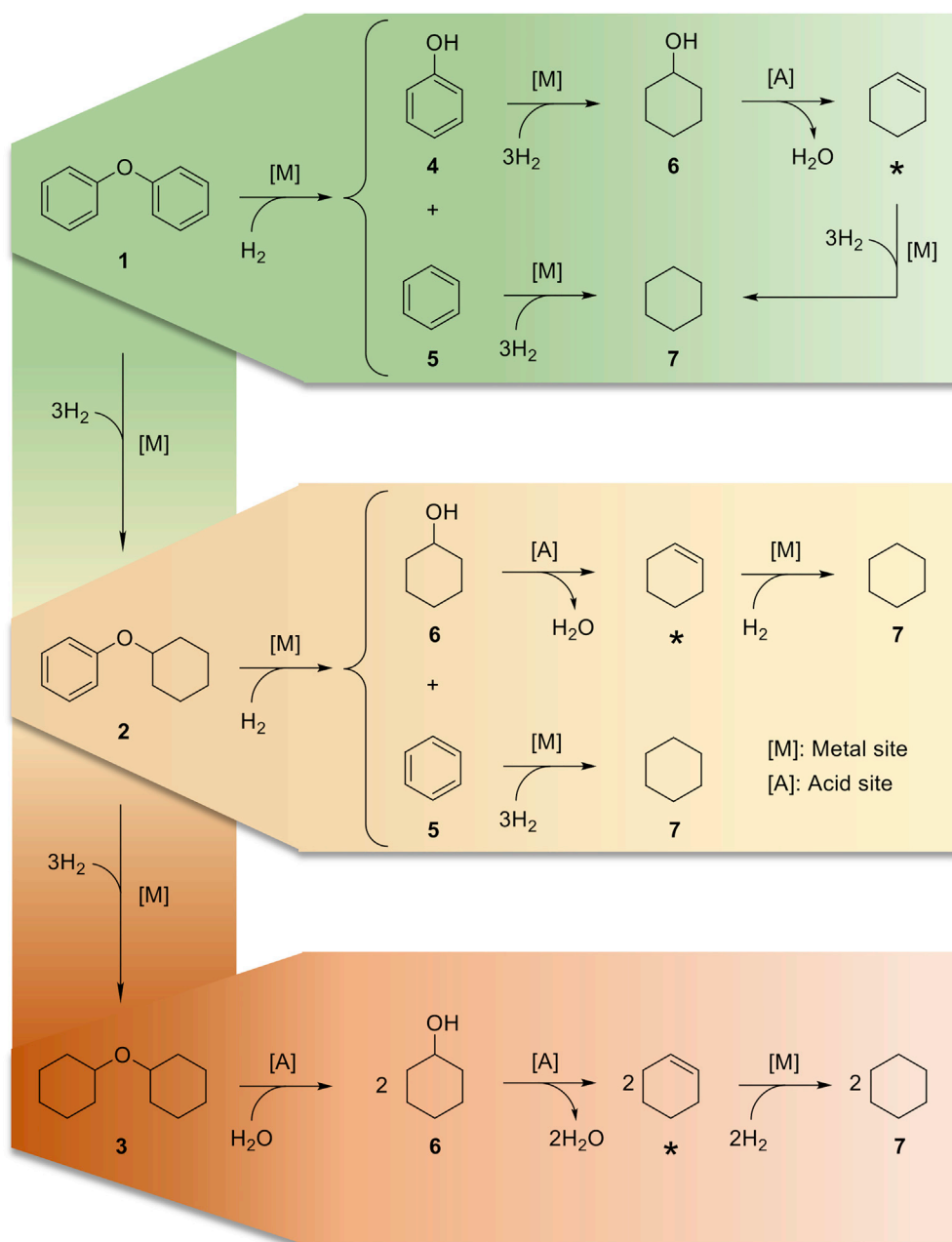


Figure 5. Reaction Pathways Proposed for the Hydrotreating of Diphenyl Ether into Cyclohexane in the Presence of a Bifunctional Catalyst ([M] and [A] Stand for Metal and Acid Sites, Respectively)

In the reaction network, three ether linkages, with distinct reactivities toward hydrogenolysis catalyzed by Ni sites, are formed. The progressive saturation of diphenyl ether reduces the reactivity of the ether linkage toward hydrogenolysis over Ni sites (He et al., 2012). Noteworthy, Ni catalysts are typically inactive for the cleavage of dialkyl ethers. Thereby, the hypothetical pathway for the HDO of dicyclohexyl ether will require acid sites to start and proceed via hydrolysis \rightarrow dehydration \rightarrow hydrogenation to yield cyclohexane. This pathway is, however, not followed under the reaction conditions of this study. In this manner, dicyclohexyl ether accumulated in the reaction mixtures. For clarity, cyclohexene was not numbered but indicated by an asterisk, as this intermediate is consumed upon its formation so that it is not detected in the reaction mixtures.

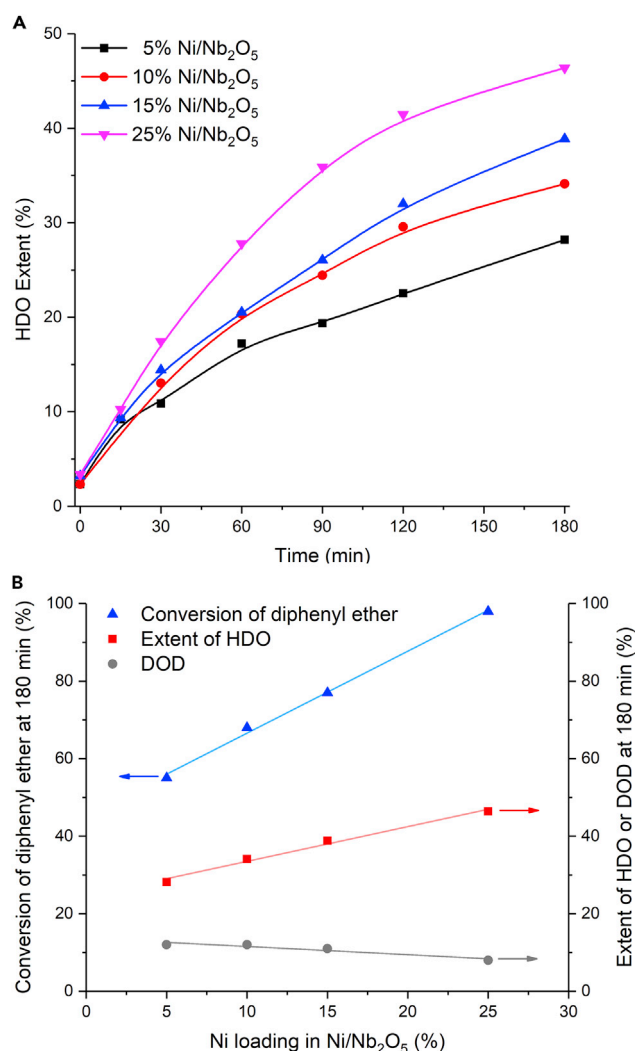


Figure 6. Evaluation of Ni/Nb₂O₅ Catalysts in the Conversion of Diphenyl Ether at 160°C

(A and B) (A) HDO extent as a function of time (note that measurement began upon the reaction mixture reaching the temperature of 160°C, ca. 15 min ramp time); (B) relationships between conversion or HDO extent or DOD and Ni loading in Ni/Nb₂O₅. Reaction conditions: diphenyl ether (13.5 mmol), *n*-dibutyl ether (3.64 mmol, as an internal standard for gas chromatography, GC, analysis), methylcyclohexane (70 mL, solvent), catalyst (0.500 g), H₂ pressure of 4 MPa (at room temperature), stirring rate of 400 rpm.

To examine in more detail the results of the experiments conducted at 160°C, the product distribution at a similar conversion level of about 50%–60% was analyzed (Table 3). Two critical ratios of products' groups were considered. The ratio $\Sigma(4-7)/\Sigma(2,3)$ was used to define the selectivity to monocyclic products produced by the cleavage of the C–O ether bond. The ratio $\Sigma(5,7)/\Sigma(4,6)$ indicates the selectivity to HDO after ether bond cleavage, which reflects the ability of the catalyst to execute the following reaction sequence: phenol → cyclohexanol → cyclohexene → cyclohexane. Evolution of the product selectivity with time at 160°C is given in Figure S3.

Table 3 shows that diphenyl ether was converted into three main products: cyclohexyl phenyl ether (22%–25%), cyclohexanol (29%–36%), and cyclohexane (27%–38%). Small quantities of dicyclohexyl ether, phenol, and benzene were also found in the reaction mixture (individual selectivity values lower than 11%). $\Sigma(4-7)/\Sigma(2,3)$ ratio higher than 1 was observed for all the Ni/Nb₂O₅ catalysts. This observation indicates the formation of monocyclic products to prevail over the partial or full saturation of diphenyl ether. The latter renders the bicyclic products 2 and 3, respectively. With the rise in Ni content in

Catalyst	Conversion (%)	Time (min)	Selectivity (%)							$\frac{\sum(4-7)}{\sum(2,3)}$	$\frac{\sum(5,7)}{\sum(4,6)}$	HDO Extent (%)	DOD (%)
			2	3	4	5	6	7					
5%Ni/Nb ₂ O ₅	55	180	23	5	1	4	29	38	2.57	1.40	28	12	
10%Ni/Nb ₂ O ₅	51	90	25	5	1	4	32	33	2.33	1.12	24	8	
15%Ni/Nb ₂ O ₅	56	90	25	6	1	4	33	31	2.23	1.03	26	7	
25%Ni/Nb ₂ O ₅	63	60	22	11	1	3	36	27	2.03	0.81	28	5	

Table 3. Product Distribution, HDO Extent, and Degree of Deoxygenation (DOD) at Iso-Conversion for the Diphenyl Ether HDO at 160°C

Ni/Nb₂O₅ catalysts (from 5 to 25 wt %), a gradual reduction in the $\Sigma(4-7)/\Sigma(2,3)$ ratio (from 2.57 to 2.03) was observed. Taking the results from the experiment carried out in the presence of 25 wt % Ni/Nb₂O₅ catalyst into account, the reduction in the $\Sigma(4-7)/\Sigma(2,3)$ ratio is related to the accumulation of dicyclohexyl ether in the reaction mixture. As previously reported, dialkyl ethers are not prone to undergo hydrogenolysis in the presence of Ni catalysts under relatively mild reaction conditions (Wang and Rinaldi, 2016; Zhao et al., 2012a). Should a dialkyl ether be cleaved, the reaction pathway would begin with a hydrolysis step instead (Figure 5). However, in this study, the formation of dicyclohexyl ether constitutes a dead end, as its conversion was not observed. Confirming this, we could successfully employ *n*-dibutyl ether in the reaction mixtures as an internal standard for gas chromatography (GC) analysis. Likewise, no decomposition of the internal standard was detected.

The results in Table 3 also shows a rise in the selectivity to cyclohexanol (from 6% to 11%) for the experiment carried out in the presence of 25 wt % Ni/Nb₂O₅ catalyst. This outcome agrees with the decrease in Brønsted acidity at a high Ni content supported on Nb₂O₅, as verified by ATR-IR spectra of pyridine adsorbed on the reduced Ni/Nb₂O₅ catalysts (Figure 4) and model reaction experiments (dehydration of cyclohexanol, Table 2). Therefore, the increase in Ni loading on Nb₂O₅ has implications for both the accumulation of dicyclohexyl ether (i.e., raises the likelihood of full saturation of diphenyl ether to dicyclohexyl ether) and of cyclohexanol (i.e., lessens the extent of dehydration of cyclohexanol).

The product distributions in Table 3 show similar values of selectivity to cyclohexanol and cyclohexane, revealing that Nb₂O₅ plays a marginal role in the HDO extent at 160°C. Under these conditions, low DOD values (5%–12%) were achieved. The catalyst's ability to dehydrate cyclohexanol significantly reduces with the rise in Ni content, as indicated by the decrease in the $\Sigma(5,7)/\Sigma(4,6)$ ratio from 1.40 to 0.81. The decrease in the dehydration capability is correlated with the decrease in the number of Brønsted acid sites with the increase in Ni content, as discussed in the previous section.

According to the results from Table 3, 10%Ni/Nb₂O₅ and 15%Ni/Nb₂O₅ catalysts present the best balance between HDO extent and selectivity to monocyclic deoxygenated products. These catalysts were thus chosen for the conversion of diphenyl ether carried out at 200°C. Figure 7 shows the monitoring of the reaction mixture components over time. For both experiments, full conversion was achieved at 180 min. Cyclohexane was the main product obtained, with selectivity values of 81% and 88% for the 10%Ni/Nb₂O₅ and 15%Ni/Nb₂O catalysts, respectively. These results confirm that the dehydration of cyclohexanol is encouraged at 200°C. At 180 min, the HDO extent and DOD were both greater for 15%Ni/Nb₂O₅ (HDO extent: 91%; DOD: 85%) than for the 10%Ni/Nb₂O₅ catalyst (HDO extent: 82%; DOD: 72%). Based on these results, 15%Ni/Nb₂O₅ catalyst was considered as the most efficient. Thus the 15%Ni/Nb₂O₅ catalyst was selected for the recycling experiments and studies on the conversion of lignin oil.

The catalytic performance after five reaction cycles was investigated for the HDO of diphenyl ether at 200°C for 240 min using the 15%Ni/Nb₂O₅ catalyst. Again, diphenyl ether serves as a model compound because,

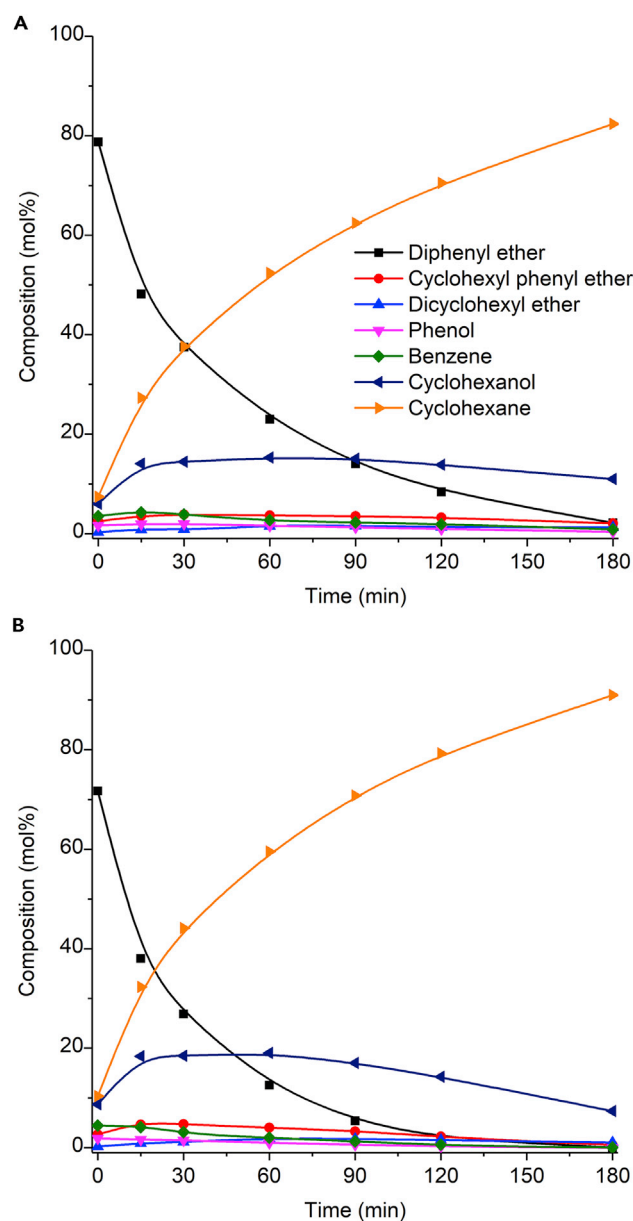


Figure 7. Catalytic Conversion of Diphenyl Ether at 200°C

Monitoring of reaction mixture composition for the conversion of diphenyl ether at 200°C in the presence of (A) 10%Ni/Nb₂O₅ or (B) 15%Ni/Nb₂O₅ catalyst. Reaction conditions: diphenyl ether (13.5 mmol), *n*-dibutyl ether (3.64 mmol, as an internal standard for GC analysis), methylcyclohexane (70 mL, solvent), catalyst (0.500 g), H₂ pressure of 4 MPa (at room temperature), and stirring rate of 400 rpm. Note that time measurement began upon reaching a temperature of 200°C (ca. 20 min ramp time).

when targeting the full HDO of lignin streams, the accumulation of cyclohexanol (derived from hydrogenation of phenol) indicates a decay of the initial acidic properties of a bifunctional catalyst. After each reaction run, the catalyst was washed with solvent and reused in the following reaction run. Figure 8 displays the conversion and product distribution after each reaction run.

Figure 8 shows that the catalyst presents a sustained performance, still producing a 91% yield of cyclohexane after five reaction runs. A slight decrease in the cyclohexane selectivity is, however, observed from the second to fourth reaction runs, with the formation of cyclohexanol and dicyclohexyl ether (around

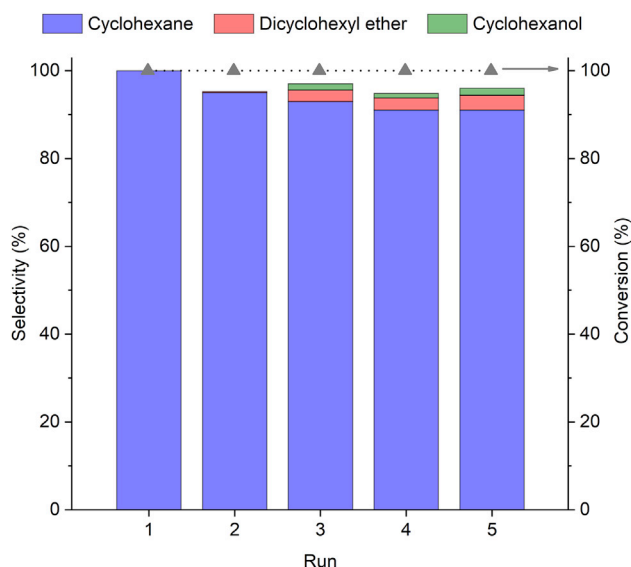


Figure 8. Sustained Catalyst Performance of 15% Ni/Nb₂O₅ in the Recycling Experiments at 200°C

Performance of 15%Ni/Nb₂O₅ in the conversion of diphenyl ether at 200°C throughout the recycling experiments. Reaction conditions for each cycle: diphenyl ether (13.5 mmol), *n*-dibutyl ether (3.64 mmol, as an internal standard for GC analysis), methylcyclohexane (70 mL, solvent), catalyst (0.500 g), H₂ pressure of 4 MPa (at room temperature), reaction time of 240 min, and stirring rate of 400 rpm. Note that time measurement began upon reaching a temperature of 200°C (ca. 20 min ramp time).

4%–5% each) from the third cycle on. These results translate into a slight decrease in both HDO extent (from 100% to 92%) and DOD (from 100% to 94%) throughout the recycling experiments.

To examine surface, structural, and morphological alterations occurring in the 15%Ni/Nb₂O₅ catalyst, the fresh and spent catalysts were analyzed by using a set of techniques (pyridine adsorption, XRD, and HAADF-STEM). Figure 9 shows the ATR spectra of adsorbed pyridine on the fresh catalysts and spent samples after five reaction runs. The data indicates that the population of Brønsted acid sites dramatically decreased after five successive reuses of the catalyst. This means that even though water is generated during the reaction, no regeneration of Brønsted acidity takes place in the process. In this context, the accumulation of cyclohexanol appears to be related to a decrease in the population of Brønsted acid sites. On the other hand, Lewis acidity is preserved, which explains the sustained high selectivity to cyclohexane at 200°C, demonstrating that Nb₂O₅ Lewis acid sites are stable under the reaction conditions. Moreover, a modest decrease in BET surface area was observed (fresh catalyst: 180 m² g⁻¹ versus spent catalyst: 144 m² g⁻¹). The XRD pattern of the used catalyst (Figure 10) also shows that the crystalline structure of the catalyst is maintained after five reaction runs. Also, no significant change in the Ni average crystallite size occurred after five reaction runs (fresh catalyst: 14 nm versus spent catalyst: 15 nm). Finally, the comparison of STEM-HAADF images (Figure 11) indicates that the spent catalyst after the fifth reaction run maintains the original features of the fresh catalyst, that is, the arrangement and size distribution of Ni nanoparticles entangled in the Nb₂O₅ nanorod nest remained, to a great extent, unaltered. Overall, these observations together with the sustained catalytic performance of the 15%Ni/Nb₂O₅ indicated that this material holds potential as a robust and active catalyst for the conversion of phenolic streams derived from lignin.

Hydrodeoxygenation of Lignin Oil

To explore the potential of 15%Ni/Nb₂O₅ catalyst in the conversion of lignin oil, lignin oil was subjected to hydrotreatment under an H₂ pressure of 7 MPa (measured at room temperature) at 300°C for 16 h. We chose to increase the reaction temperature from 200°C (as for the model compound experiments) to 300°C to encourage extensive HDO of lignin oil to cycloalkanes, leading to full conversion of lignin into products soluble in *n*-pentane (reaction solvent), thus avoiding the accumulation of lignin residues throughout the catalyst recycling experiments (Wang and Rinaldi, 2012). However, even under harsh conditions, an appreciable amount of a residue insoluble in *n*-pentane or even methanol (a good solvent for

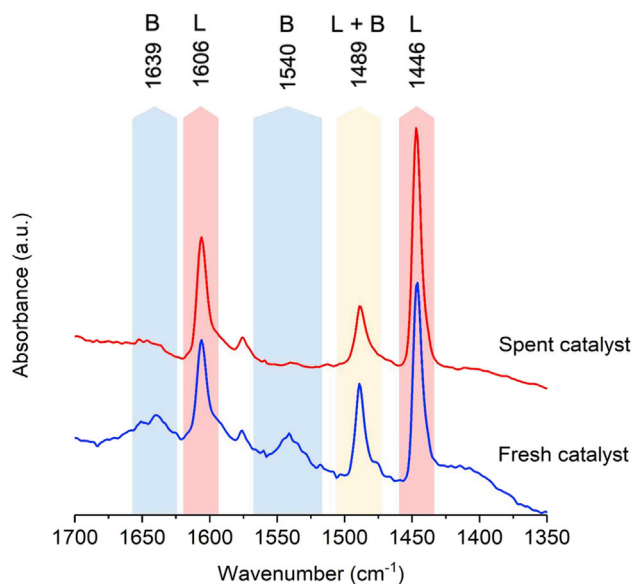


Figure 9. ATR-FTIR Spectrum of Pyridine Adsorbed on the Catalyst 15%Ni/Nb₂O₅ before and after Five Reaction Runs

lignin oil species) was formed and, thus, accumulated with the catalyst. Thereby, in this study, the “conversion of lignin oil” is estimated as a “net conversion,” which takes into account the weight of residue insoluble in either *n*-pentane or methanol formed in each reaction run (in conjunction with the initial weight of fresh catalyst) and the amount of lignin oil added in each reaction run. For the catalyst recycling experiments, the spent catalyst was washed with methanol to extract soluble residue species. The spent catalyst containing lignin-derived residues insoluble in methanol was then recovered by filtration and dried at 40°C in a vacuum oven. The liquid products and the fraction of lignin residues soluble in methanol were characterized by elemental analysis, gas chromatography (GC)-flame ionization detector (FID)/mass spectrometry (MS), and gel permeation chromatography (GPC).

Throughout the catalyst recycling experiment, which processed in total ca. 6.0 g of lignin oil, the amount of lignin-derived residue increased from ca. 0.23 g (first run) to 0.30–0.31 g (second or third run, Table 4). Logically, the accumulation of the lignin-derived residue impedes the precise determination of the initial quantity of substrate present in the second and third reaction runs, as it is not possible to discern whether a part of the lignin-derived residue was also consumed throughout the recycling experiment and replaced with a fresh, more oxygenated carbonaceous residue derived from the fresh substrate. Further exploration of the data listed in Table 4, that is, the determination of weight ratio of liquid-product-to-residue, should be carried out with caution. A mass ratio of liquid-product-to-residue is only meaningful if both liquid product and residue present similar values of O/C and H/C ratios, which is not the case when the catalyst loses part of its performance in the recycling experiments.

Figure 12 summarizes in a van Krevelen diagram the results obtained from the control experiment and catalyst recycling in the hydrotreating of lignin oil. In the absence of the catalyst, a 68% conversion of the lignin oil was achieved by thermal processes (Table 4), increasing the H/C ratio from 1.51 ± 0.01 , for the lignin oil, to 1.74 ± 0.02 for the liquid fraction. Conversely, the O/C ratio decreased from 0.46 ± 0.01 , for the lignin oil, to 0.23 ± 0.01 for the produced liquid fraction. This decrease in O/C ratio is associated with the elimination of the γ -OH group of *p*-dihydrolignols, among other thermal processes, leading to deoxygenation (Table S4). The solid residue exhibited an H/C ratio of 1.45 ± 0.03 and an O/C ratio of 0.34 ± 0.01 . These results indicate that the residue no longer corresponds to the initial lignin stream.

In the catalytic experiments, an 89% conversion of lignin in the first reaction run was achieved. For the liquid product obtained from the first reaction run, a substantial increase in the H/C ratio from 1.51 ± 0.01 , for the lignin oil, to 1.80 ± 0.01 was achieved. In parallel, the O/C molar ratio decreased from 0.46 ± 0.01 to 0.006 ± 0.004 for the liquid product. These results demonstrate the extensive removal of oxygen and incorporation of hydrogen in the liquid product. In the subsequent catalyst reuse, the net conversion of lignin oil

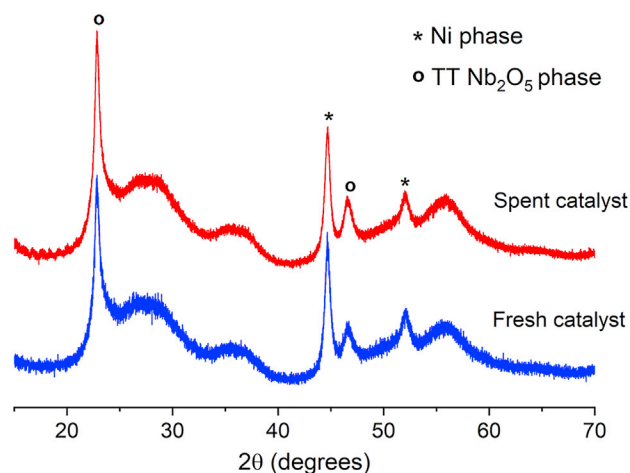


Figure 10. XRD Pattern for the 15%Ni/Nb₂O₅ before and after Five Reaction Runs

slightly decreased from 89% to 85%, for both the second and third reaction runs (Table 4). For the liquid products, H/C ratios of 1.76 ± 0.01 and 1.75 ± 0.03 for the second and third reaction runs, respectively, were obtained. These values are slightly lower than those of the liquid products from the first reaction run ($H/C: 1.80 \pm 0.01$). On the other hand, O/C ratios substantially increased from 0.006 ± 0.004 , for the first reaction run, to 0.14 ± 0.01 and 0.16 ± 0.01 , for the second and third reactions runs, respectively. For the residue fraction soluble in MeOH, which corresponds to ca. 10% of the lignin-derived residues, the H/C ratio decreased from 1.73 ± 0.01 (first reaction run) to 1.62 ± 0.01 and 1.62 ± 0.06 , for the second and third reaction runs, respectively. In parallel, O/C ratios rose from 0.29 ± 0.04 (first reaction run) to 0.33 ± 0.01 and 0.36 ± 0.01 for the second and third reaction runs, respectively. Altogether, the O/C and H/C ratios found for the liquid products and residues indicate that the catalyst's hydrogenation activity deteriorated to an extent lesser than that of the deoxygenation ability.

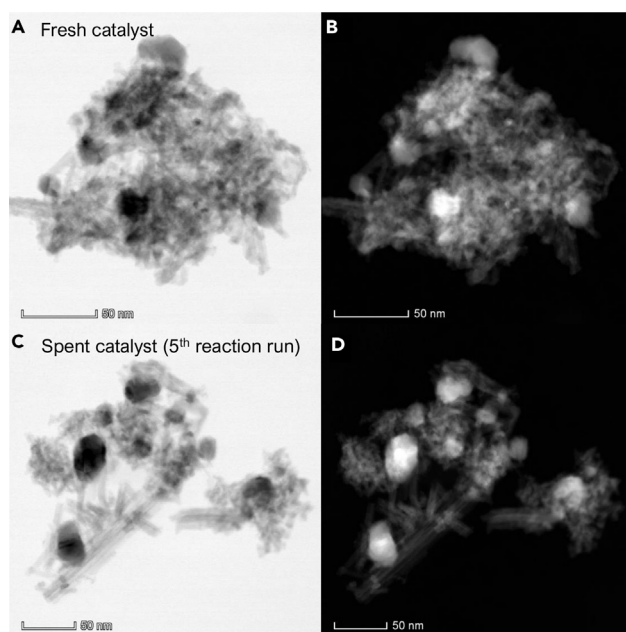


Figure 11. HAADF-STEM Images of 15%Ni/Nb₂O₅ before and after Five Reaction Runs

HAADF-STEM images of (A and B) fresh 15%Ni/Nb₂O₅ catalyst, and (C and D) spent 15%Ni/Nb₂O₅ catalyst after five reaction runs. Images (B) and (D) correspond to the ratio of high-angle to low-angle ADF signal.

Reaction	Weight (g)			Net Conversion (%)
	Liquid Product	Residue Insoluble in <i>n</i> -Pentane and Methanol	Residue Soluble in Methanol	
1 st Run	0.2941	0.2293	0.0249	89
2 nd Run	0.8663	0.2990	0.0204	85
3 rd Run	0.5907	0.3085	0.0240	85

Table 4. Overall Results for the HDO of Lignin Oil in the Recycling Experiments

Reaction conditions for each cycle: lignin bio-oil (2 g), *n*-pentane (100 mL, solvent), 15%Ni/Nb₂O₅ catalyst (initial weight: 0.400 g), H₂ pressure of 7 MPa (at room temperature), 16 h at 300°C, stirring rate of 400 rpm.

To gain an in-depth insight into the composition of the volatile fraction of the liquid products, GC-FID/MS analysis was carried out (Figure 13). In the volatile fraction of the lignin oil (corresponding to 28% at an injector temperature of 300°C), the main components were *p*-dihydrolignols [4-(3-hydroxypropyl)-2-methoxyphenol and 4-(3-hydroxypropyl)-2,6-dimethoxyphenol, Table S4] followed by other alkylphenol compounds. In the control experiment, thermolytic processes on the *p*-dihydrolignols caused the elimination of γ -OH group, rendering 4-propylguaiaicol and 4-propylsyringol. Other products from the cracking of the propyl side chain were formed (Table S4). At a much lesser extent, cyclohexanols (6.6%) and cycloalkanes (1.3%) were also formed. In the presence of 15%Ni/Nb₂O₅ catalyst, the primary volatile products were cycloalkanes (47%) and cyclohexanols (2%). Half of the cycloalkanes' fraction content corresponded to bicyclic aliphatic compounds. In the catalyst recycling, the content of cycloalkanes in the liquid product significantly decreased from 47%, for the fresh catalyst, to 8% and 5%, for the second and third reaction runs, respectively. As a result, the dominant species in the liquid products became cyclohexanols (31%–35%). The high content of monophenolic species (18–19%) reveals that the catalyst's hydrogenation ability was also impaired after the first use of the catalyst. However, the catalyst hydrogenation ability was affected to an extent lesser than that for the dehydration of cyclohexanol intermediates.

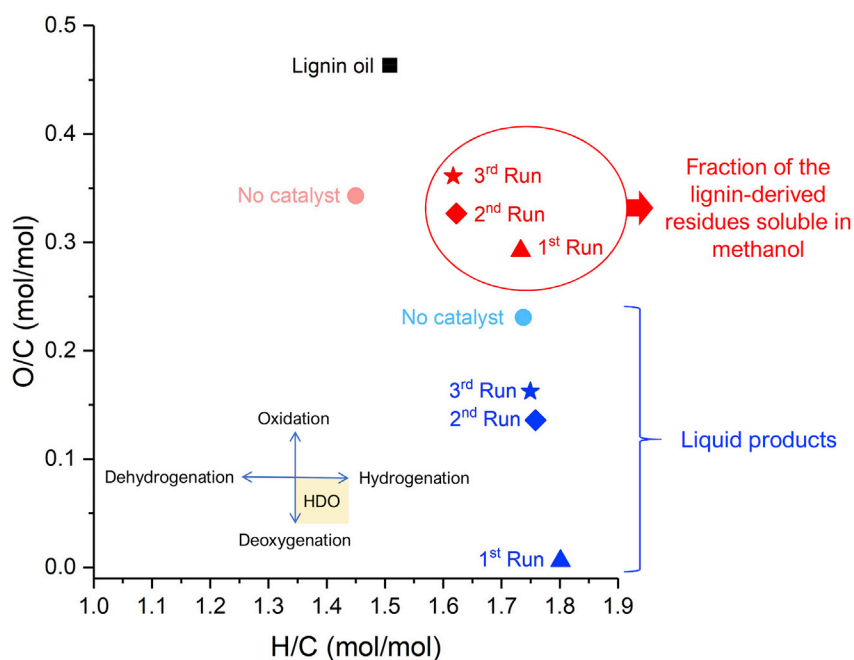


Figure 12. Snapshot of the HDO Performance of 15%Ni/Nb₂O₅ Catalyst in the Recycling Experiments

van Krevelen plot comparing the H/C and O/C molar ratios for the lignin oil, residue fraction soluble in methanol, and liquid products obtained in the presence of 15%Ni/Nb₂O₅ catalyst and from the control experiment (no added catalyst).

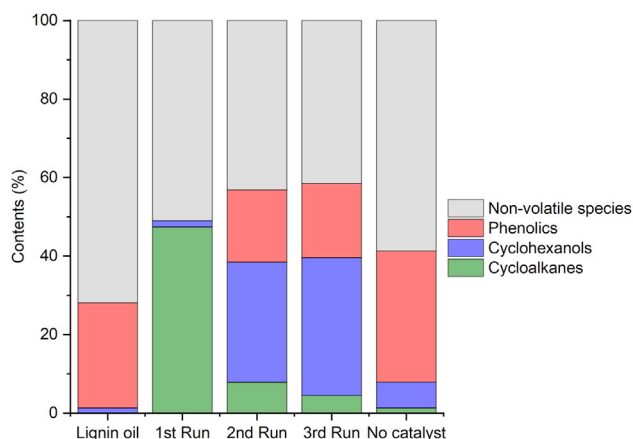


Figure 13. Distribution of compound classes in lignin oil and processed streams

Comparison of distributions of compound classes in the lignin oil, liquid products from the hydroprocessing of lignin oil in the presence of the 15%Ni/Nb₂O₅ catalyst, and control experiment (no added catalyst). Reaction conditions for each cycle: lignin bio-oil (2 g), *n*-pentane (100 mL, solvent), catalyst (0.400 g), H₂ pressure of 7 MPa (at room temperature), 16 h at 300°C, stirring rate of 400 rpm.

To assess the extent of decrease in the acidity of the Nb₂O₅ support, ATR-IR measurements of pyridine adsorbed on the spent 15%Ni/Nb₂O₅ catalyst were performed. After the third reaction run, Figure 14 reveals that the spent catalyst no longer presents either Brønsted or Lewis acid sites accessible to pyridine adsorption. These results demonstrate the decrease in the deoxygenation activity of 15%Ni/Nb₂O₅ to be caused by the blocking of acid sites on the Nb₂O₅ support. Surprisingly, despite the loss of acidity, the structural properties of the Nb₂O₅ nanorods were not affected upon recycling (as shown by XRD pattern features, Figure S4). By stark contrast, the size of the Ni particles increased from 14 to 80 nm after three reaction runs (Figure S4). Thereby, the decrease in the hydrogenating activity of the catalyst appears to be related to the decrease in metal surface area due to Ni particle growth.

From the data presented in Figure 13, the sum of compounds visible by the GC technique corresponds to approximately half of the content of species occurring in the liquid products. To expand our analysis toward the heavy species, GPC was performed on the hydrotreated liquid products and residue fractions soluble in methanol. Noteworthy, when applied to product mixtures obtained from lignin, direct information regarding the content of species cannot be retrieved from an ultraviolet-visible (UV-vis) detector (in this study, a photodiode array [PDA] detector), as the detector response is not universal. Furthermore, in samples containing aliphatic hydrocarbons, these compounds will be invisible to the UV-vis detector. Despite these limitations, the GPC technique coupled with UV-vis spectroscopy provides useful information on the apparent distribution of *M_w* and spectral signature of the eluting species. Figure 15 displays the chromatogram traces at a wavelength of 280 nm.

Figure 15 shows that the lignin oil substrate encompasses species of apparent *M_w* from 100 to 66,000 Da. In the absence of the 15%Ni/Nb₂O₅ catalyst (control experiment), thermal processes on lignin generate soluble species of *M_w* lower than 1,200 Da for both the product oil and solid residues, at the expense of the heavy species. In the presence of the fresh 15%Ni/Nb₂O₅ catalyst, both the liquid product and the residue fraction soluble in methanol still contain UV-absorbing species heavier and of much broader apparent *M_w* distributions, compared with those from the control experiment. Surprisingly, the subsequent reaction runs yielded liquid products and residues of an apparent *M_w* distribution comparable to the apparent *M_w* range of products formed in the control experiment.

To gain further information about the chemical nature of the UV-absorbing species, the spectral data collected by the PDA detector in the GPC analysis was examined in detail (Figure 16). In the samples from the first reaction run, a key feature distinguishing the PDA images is the presence of species absorbing at wavelengths higher than 300 nm for the residue fraction soluble in methanol (indicated in Figure 16 by a yellow-coded dotted line). In lignin chemistry, this spectral feature is often related to the presence of quinone methide intermediates, stilbene species, and other conjugated unsaturated species

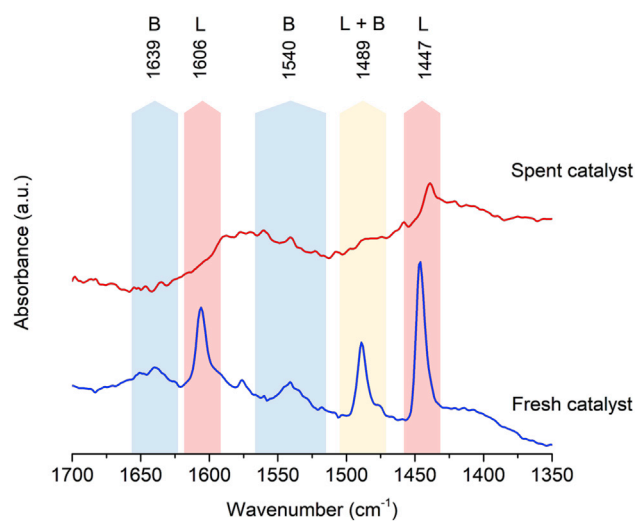


Figure 14. ATR-FTIR Spectra of Pyridine Adsorbed on the 15%Ni/Nb₂O₅ Catalyst before and after Recycling (Third Run)

associated with lignin condensation processes (Lin, 1992; Schmidt, 2010). Overall these observations suggest that, in the presence of the fresh 15%Ni/Nb₂O₅ catalyst, the condensation of lignin species could not entirely be suppressed by the reductive processes, as the former process appears to take place at a rate faster than the latter. Interestingly, similar PDA images are found for both liquid products and the residues soluble in methanol from the second and third reaction runs. These images show no strong absorption spot at wavelengths higher than 300 nm. Altogether, these observations support the hypothesis that Lewis acid sites of Nb₂O₅ play a role in the condensation of lignin species. As these sites become largely blocked in the first reaction run, the condensation of lignin species should occur to a lesser extent in the subsequent reaction runs. This hypothesis appears to be plausible also considering that the weight of lignin residue accumulated with the catalyst plateaued after the second reaction run (Table 4).

Conclusions

This study provided a beginning-to-end analysis of the multifaceted picture of the design of water-tolerant catalysts for the hydrotreating of lignin streams. From the observations of this study, the following conclusions and recommendations for future research are given:

1. In the design of bifunctional Ni/Nb₂O₅, the incorporation of the Ni phase reduces the population of Brønsted acid sites. However, the population of Lewis acid sites remained almost unaltered. The dehydration of cyclohexanol over Brønsted acid sites takes place at temperatures lower than those required for the reaction catalyzed by Lewis acid sites. By employing the hydrotreating of diphenyl ether to cyclohexane as a model reaction, it was possible to find a compromise between hydrogenation and dehydration catalyst's capabilities, thus taking the benefit from the catalyst Lewis acidity for the hydrotreatment. The 15%Ni/Nb₂O₅ catalyst showed sustained results in the recycling experiments. As a result of the high stability of the water-resistant Lewis acid sites, a 91% yield of cyclohexane could be achieved even after five reaction runs.
2. Despite the promising results achieved in the hydrotreatment of diphenyl ether, the 15%Ni/Nb₂O₅ catalyst lost its activity toward dehydration of the cyclohexanol species already after the first reaction run performed on the lignin oil stream. This disappointing outcome is associated with the blocking of the Lewis acid sites.
3. In the current literature on lignin hydroprocessing, little attention has been given to the fact that the acid sites, needed for the dehydration of cyclohexanol species, can also catalyze the condensation of lignin oligomeric species. In this study, we demonstrated that lignin condensation occurs even under reductive conditions and when beginning the process with passivated streams from the lignin-first biorefining based on reductive processes.

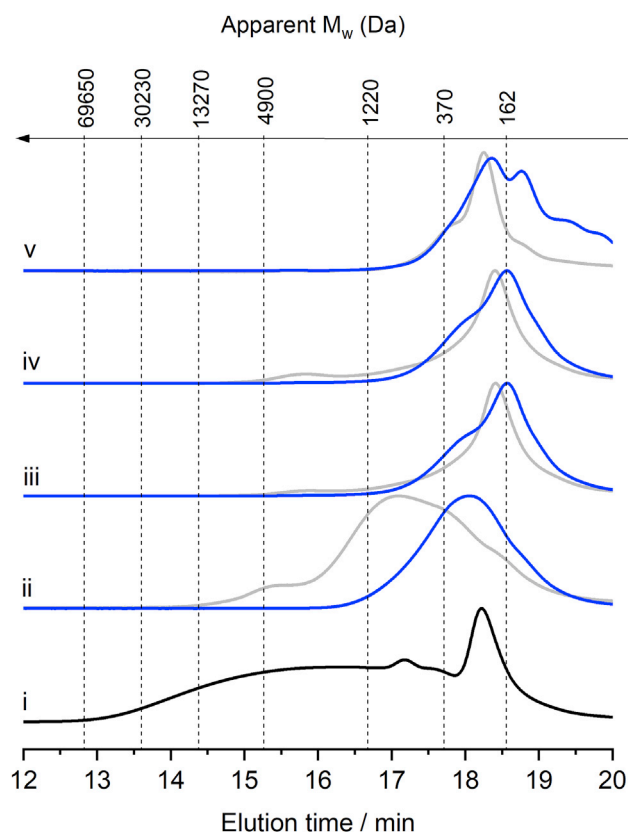


Figure 15. Gel Permeation Chromatogram Traces at a Wavelength of 280 nm

Gel permeation chromatograms for the (i) lignin oil, liquid products (blue-coded curves) and solid residues (gray-coded curves) obtained from the process with added catalyst in the (ii) first reaction run, (iii) second reaction run, and (iv) third reaction run, and (v) control experiment with no added catalyst. The apparent M_w is given relative to polystyrene standards. Signal intensities of the curves are not scaled.

- The condensation of lignin catalyzed by Nb_2O_5 nanorods' Lewis acid sites appears to be a chemical process faster than the saturation or HDO of lignin species. As a result, in the presence of Ni/Nb_2O_5 catalysts, lignin condensation is not entirely suppressed by reductive processes. Consequently, carbonaceous matter is formed, blocking the Lewis acid sites.
- Previous studies on hydrotreating of lignin oils in the presence of phosphided Ni/SiO_2 catalysts demonstrated that recyclable hydrotreating catalysts could be produced (Cao et al., 2018; Samec, 2018). Confronting those results with the current ones, it is concluded that the control of the surface acidity is mandatory for the success of lignin oil hydrotreating. Further research is required to define the type of acidity and a threshold of acidity required for the hydrotreating of lignin while not encouraging acid-catalyzed condensation processes on the lignin oligomeric species. Surprisingly, such a research line has not been receiving much attention from the community. Indeed, often studied model compounds (e.g., diphenyl ether, benzyl phenyl ether, (alkyl)guaiacols, and several others) cannot undergo condensation reactions. Therefore, the crucial role of lignin condensation in hydrotreating processes cannot be mimicked by the current set of model compounds employed in this research field. This fact clearly limits the translation of technologies designed for the HDO of model compounds to the hydrotreating of real-world lignin streams.
- The balance of dehydration and hydrogenation abilities of a heterogeneous catalyst becomes a very complicated issue when considering the significant impact of lignin condensation throughout the hydrotreating process. Considering this, a tentative solution could be the utilization of two solid catalysts, one for hydrogenation and another one for dehydration, so that the balance of these specific tasks could be then more easily adjusted by the weight ratio of each catalyst component in the mixture of catalysts. This idea has been already exploited with success (Wang and Rinaldi, 2013).

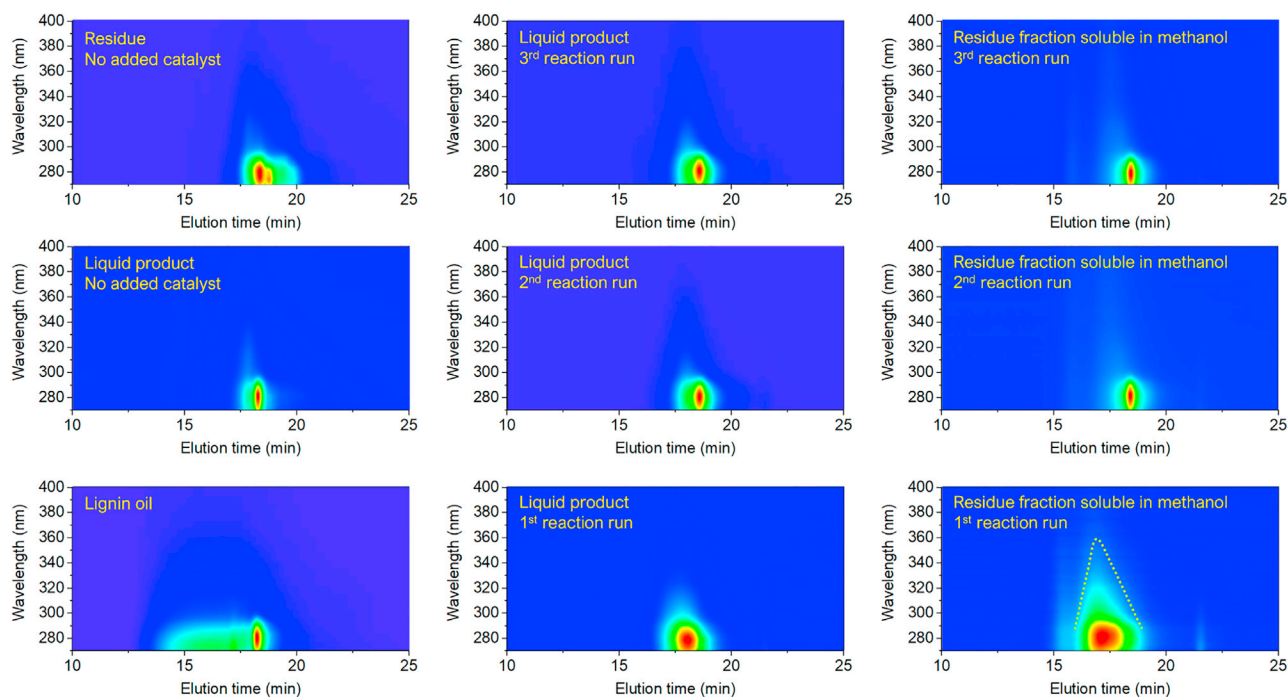


Figure 16. Spectral Signature of the Eluting Species in the GPC Analysis

PDA detector response images for the eluting species in the GPC analysis performed on lignin oil, liquid products, and residues obtained with no added catalyst (control experiment) and in the presence of 15%Ni/Nb₂O₅ catalyst (recycling experiment). The yellow-coded dotted line in the PDA image of the solid residue (first reaction run) indicates the extension of the UV-vis absorption signal.

However, the conversion of a batch reaction process to a continuous flow process based on a mixture of catalysts constitutes a challenging task. A more practical approach appears to be the combination of flow-through reactors operating in series but at different temperatures. This approach could circumvent catalyst deactivation by the formation of coke via lignin condensation, by gradually saturating the lignin stream under conditions of gradual increase in process severity. A similar approach was demonstrated to be very fruitful for the hydrotreatment of pyrolysis oil in the presence of Ni-Cu catalysts (Yin et al., 2016).

In a broader context, this work provides substantial evidence that the use of model reactions has severe limitations for the design of catalysts for the hydroprocessing of lignin streams. Accordingly, the catalyst screening carried out on real-world lignin streams is a more productive enterprise to pursue, regardless of the complexity of the product mixtures obtained. In this quest, the evaluation of H/C and O/C ratios as the response variables (either for the catalyst discovery or in recycling experiments) constitutes a strategy effective in the simplification of characterization procedures applied to the lignin products. Such a strategy should become a gold standard in the high-throughput screening catalysts for the hydroprocessing of lignin streams to produce drop-in lignin biofuels, as it allows for the direct comparison of catalyst performance without the need of scrutinizing the lignin product compositions at an early stage of technology-readiness levels (TRL), thus contributing to accelerating catalyst discovery.

Limitations of the Study

The hydrothermal synthesis of Nb₂O₅ is based on the decomposition of niobium peroxy species formed by the reaction of ammonium niobium(V) oxalate and hydrogen peroxide. **CAUTION:** As the hydrothermal synthesis is performed in a closed stainless-steel vessel, it is mandatory to check if the vessel is rated to operate under the pressure built by the decomposition of the full content of hydrogen peroxide employed in the synthesis.

METHODS

All methods can be found in the accompanying [Transparent Methods supplemental file](#).

SUPPLEMENTAL INFORMATION

Supplemental Information can be found online at <https://doi.org/10.1016/j.isci.2019.05.007>.

ACKNOWLEDGMENTS

R.R. acknowledges the financial support provided by the ERC Consolidator Grant LIGNINFIRST (Project Number: 725762). R.R. and A.A.S.C. thank FAPESP for the support provided (Process Number: 2016/50423-3). The authors are grateful to LNLS/CNPEM for the infrastructure (XPD beamline and chemistry laboratory), LNNano for the STEM infrastructure, the GPMML laboratory (IQ-UNICAMP) for the quantitative FTIR of adsorbed pyridine analysis, CNPq for the PhD scholarship (Process Number: 165106/2014-0), and CAPES for the PDSE scholarship (Process Number: 88881.132245/2016-01). This study was financed in part by the Coordenação de Aperfeiçoamento de Pessoal de Nível Superior - Brasil (CAPES) - Finance Code 001. Finally, the authors are thankful to CBMM for the ammonium niobium oxalate hydrate samples.

AUTHOR CONTRIBUTIONS

Conceptualization, G.F.L, A.A.S.C., and R.R.; Methodology, G.F.L. and R.R.; Investigation, G.F.L., I.G., S.L., H.C., D.H.B., A.A.S.C., C.B.R., E.T.-N., and R.R.; Writing – Original Draft, G.F.L.; Writing – Review & Editing, G.F.L., C.B.R., A.A.S.C., and R.R.; Funding Acquisition, C.B.R., A.A.S.C., and R.R.; Resources, C.B.R., A.A.S.C., and R.R.; Supervision, C.B.R., A.A.S.C., and R.R.

DECLARATION OF INTERESTS

The authors have no conflict of interests to declare.

Received: December 13, 2018

Revised: April 29, 2019

Accepted: May 5, 2019

Published: May 31, 2019

REFERENCES

- Ali, R.F., Nazemi, A.H., and Gates, B.D. (2017). Surfactant controlled growth of niobium oxide nanorods. *Cryst. Growth Des.* *17*, 4637–4646.
- Barrios, A.M., Teles, C.A., De Souza, P.M., Rabelo-Neto, R.C., Jacobs, G., Davis, B.H., Borges, L.E.P., and Noronha, F.B. (2017). Hydrodeoxygenation of phenol over niobia supported Pd catalyst. *Catal. Today* *302*, 115–124.
- Brayner, R., and Bozon-Verduraz, F. (2003). Niobium pentoxide prepared by soft chemical routes: morphology, structure, defects and quantum size effect. *Phys. Chem. Chem. Phys.* *5*, 1457–1466.
- Cao, Z., Dierks, M., Clough, M.T., Rinaldi, R., Cao, Z., Dierks, M., Clough, M.T., Barros, I., and De Castro, D. (2018). A convergent approach for a deep converting lignin-first biorefinery rendering high-energy-density drop-in fuels. *Joule* *2*, 1118–1133.
- Chan, X., Pu, T., Chen, X., James, A., Lee, J., Parise, J.B., Kim, D.H., and Kim, T. (2017). Effect of niobium oxide phase on the furfuryl alcohol dehydration. *Catal. Commun.* *97*, 65–69.
- Chary, K.V.R., Sri Lakshmi, K., Murthy, M.R.V.S., Rao, K.S.R., and Papadaki, M. (2003). Hydrodechlorination of 1,2,4-trichlorobenzene over niobia supported nickel catalysts. *Catal. Commun.* *4*, 531–535.
- Cui, X., Yuan, H., Junge, K., Topf, C., Beller, M., and Shi, F. (2017). A stable and practical nickel catalyst for the hydrogenolysis of C–O bonds. *Green. Chem.* *19*, 305–310.
- Datka, J. (1992). Acidic properties of supported niobium oxide catalysts: an infrared spectroscopy investigation. *J. Catal.* *135*, 186–199.
- do Prado, N.T., and Oliveira, L.C.A. (2017). Nanostructured niobium oxide synthesized by a new route using hydrothermal treatment: high efficiency in oxidation reactions. *Appl. Catal. B Environ.* *205*, 481–488.
- Dollish, F.R., Fateley, W.G., and Bentley, F.F. (1974). *Characteristic Raman Frequencies of Organic Compounds*, First Edition (Wiley).
- Dorrestijn, E., Laarhoven, L.J.J., Arends, I.W.C.E., and Mulder, P. (2000). Occurrence and reactivity of phenoxyl linkages in lignin and low rank coal. *J. Anal. Appl. Pyrolysis* *54*, 153–192.
- Ferrini, P., and Rinaldi, R. (2014). Catalytic biorefining of plant biomass to non-pyrolytic lignin bio-oil and carbohydrates through hydrogen transfer reactions. *Angew. Chem. Int. Ed.* *53*, 8634–8639.
- Foo, G.S., Wei, D., Sholl, D.S., and Sievers, C. (2014). Role of Lewis and Brønsted acid sites in the dehydration of glycerol over niobia. *ACS Catal.* *4*, 3180–3192.
- Francisco, M.S.P., Landers, R., and Gushikem, Y. (2004). Local order structure and surface acidity properties of a Nb₂O₅/SiO₂ mixed oxide prepared by the sol-gel processing method. *J. Solid State Chem.* *177*, 2432–2439.
- Galkin, M.V., and Samec, J.S.M. (2016). Lignin valorization through catalytic lignocellulose fractionation: a fundamental platform for the future biorefinery. *ChemSusChem* *9*, 1544–1558.
- Graça, I., González, L.V., Bacariza, M.C., Fernandes, A., Henriques, C., Lopes, J.M., and Ribeiro, M.F. (2014). CO₂ hydrogenation into CH₄ on NiHNaUSY zeolites. *Appl. Catal. B Environ.* *147*, 101–110.
- Graça, I., Woodward, R.T., Kennema, M., and Rinaldi, R. (2018). Formation and fate of carboxylic acids in the lignin-first biorefining of lignocellulose via H-transfer catalyzed by Raney Ni. *ACS Sustain. Chem. Eng.* *6*, 13408–13419.
- Graça, M.P.F., Meireles, A., Nico, C., and Valente, M.A. (2013). Nb₂O₅ nanosize powders prepared by sol-gel - structure, morphology and dielectric properties. *J. Alloys Compd.* *553*, 177–182.
- Guan, W., Chen, X., Jin, S., Li, C., Tsang, C.-W., and Liang, C. (2017). Highly stable Nb₂O₅-Al₂O₃ composites supported Pt catalysts for hydrodeoxygenation of diphenyl ether. *Ind. Eng. Chem. Res.* *56*, 14034–14042.
- He, J., Zhao, C., and Lercher, J.A. (2012). Ni-Catalyzed cleavage of aryl ethers in the aqueous phase. *J. Am. Chem. Soc.* *134*, 20768–20775.
- Herval, L.K.S., von Dreifus, D., Rabelo, A.C., Rodrigues, A.D., Pereira, E.C., Gobato, Y.G., de

- Oliveira, A.J.A., and de Godoy, M.P.F. (2015). The role of defects on the structural and magnetic properties of Nb₂O₅. *J. Alloys Compd.* 653, 358–362.
- Holtzberg, F., Reisman, A., Berry, M., and Berkenblit, M. (1957). Chemistry of the group VB pentoxides. VI. The polymorphism of Nb₂O₅. *J. Am. Chem. Soc.* 79, 2039–2043.
- Iizuka, T., Ogasawara, K., and Tanabe, K. (1983). Acidic and catalytic properties of niobium pentoxide. *Bull. Chem. Soc. Jpn.* 56, 2927–2931.
- Janković, B., Adnadević, B., and Mentus, S. (2008). The kinetic study of temperature-programmed reduction of nickel oxide in hydrogen atmosphere. *Chem. Eng. Sci.* 63, 567–575.
- Jasik, A., Wojcieszak, R., Monteverdi, S., Ziolk, M., and Bettahar, M.M. (2005). Study of nickel catalysts supported on Al₂O₃, SiO₂ or Nb₂O₅ oxides. *J. Mol. Catal. A Chem.* 242, 81–90.
- Jeon, S., Park, Y.M., Park, J., Saravanan, K., Jeong, H.-K., and Bae, J.W. (2018). Synergistic effects of Nb₂O₅ promoter on Ru/Al₂O₃ for an aqueous-phase hydrodeoxygenation of glycerol to hydrocarbons. *Appl. Catal. A Gen.* 551, 49–62.
- Jin, S., Guan, W., Tsang, C.W., Yan, D.Y.S., Chan, C.Y., and Liang, C. (2017). Enhanced hydroconversion of lignin-derived oxygen-containing compounds over bulk nickel catalysts through Nb₂O₅ modification. *Catal. Letters* 147, 2215–2224.
- Ko, E.I., Hupp, J.M., and Wagner, N.J. (1984). Ethane hydrogenolysis and carbon monoxide hydrogenation over niobia-supported nickel catalysts: a hierarchy to rank strong metal-support interaction. *J. Catal.* 86, 315–327.
- Ko, E.I., and Weissman, J.G. (1990). Structures of niobium pentoxide and their implications on chemical behavior. *Catal. Today* 8, 27–36.
- Kreissl, H.T., Li, M.M.J., Peng, Y.-K., Nakagawa, K., Hooper, T.J.N., Hanna, J.V., Shepherd, A., Wu, T.-S., Soo, Y.-L., and Tsang, S.C.E. (2017). Structural studies of bulk to nanosize niobium oxides with correlation to their acidity. *J. Am. Chem. Soc.* 139, 12670–12680.
- Leal, G.F., Barrett, D.H., Carrer, H., Figueroa, S.J.A., Teixeira-Neto, E., Curvelo, A.A.S., and Rodella, C.B. (2019). Morphological, structural, and chemical properties of thermally stable Ni-Nb₂O₅ for catalytic applications. *J. Phys. Chem. C* 123, 3130–3143.
- Leite, E.R., Vila, C., Bettini, J., and Longo, E. (2006). Synthesis of niobia nanocrystals with controlled morphology. *J. Phys. Chem. B* 110, 18088–18090.
- Lin, S.Y. (1992). Ultraviolet spectrophotometry. In *Methods in Lignin Chemistry*, S.Y. Lin and C.W. Dence, eds. (Springer-Verlag), pp. 217–232. https://doi.org/10.1007/978-3-642-74065-7_15.
- Liu, J.-Y., Su, W.-N., Rick, J., Yang, S.-C., Pan, C.-J., Lee, J.-F., Chen, J.-M., and Hwang, B.-J. (2016). Rational design of ethanol steam reforming catalyst based on analysis of Ni/La₂O₃ metal-support interactions. *Catal. Sci. Technol.* 6, 3449–3456.
- Liu, Y., Vjunov, A., Shi, H., Eckstein, S., Camaioni, D.M., Mei, D., Baráth, E., and Lercher, J.A. (2017). Enhancing the catalytic activity of hydronium ions through constrained environments. *Nat. Commun.* 8, 2–9.
- Lopes, O.F., Paris, E.C., and Ribeiro, C. (2014). Synthesis of Nb₂O₅ nanoparticles through the oxidant peroxide method applied to organic pollutant photodegradation: a mechanistic study. *Appl. Catal. B Environ.* 144, 800–808.
- Luisa Marin, M., Hallett-Tapley, G.L., Impellizzeri, S., Fasciani, C., Simoncelli, S., Netto-Ferreira, J.C., and Scaiano, J.C. (2014). Synthesis, acid properties and catalysis by niobium oxide nanostructured materials. *Catal. Sci. Technol.* 4, 3044–3052.
- Morais, L.A., Adán, C., Araujo, A.S., Guedes, A.P.M.A., and Marugán, J. (2017). Synthesis, characterization, and photonic efficiency of novel photocatalytic niobium oxide materials. *Glob. Chall.* 1, 1700066–1700074.
- Nakajima, K., Baba, Y., Noma, R., Kitano, M., Kondo, J.N., Hayashi, S., and Hara, M. (2011). Nb₂O₅·nH₂O as a heterogeneous catalyst with water-tolerant Lewis acid sites. *J. Am. Chem. Soc.* 133, 4224–4227.
- Nakajima, K., Noma, R., Kitano, M., and Hara, M. (2013). Titania as an early transition metal oxide with a high density of Lewis acid sites workable in water. *J. Phys. Chem. C* 117, 16028–16033.
- Nico, C., Monteiro, T., and Graça, M.P.F. (2016). Niobium oxides and niobates physical properties: Review and prospects. *Prog. Mater. Sci.* 80, 1–37.
- Nowak, I., and Ziolk, M. (1999). Niobium compounds: preparation, characterization, and application in heterogeneous catalysis. *Chem. Rev.* 99, 3603–3624.
- Parry, E.P. (1963). An infrared study of pyridine adsorbed characterization of surface. *J. Catal.* 2, 371–379.
- Parthasarathi, R., Romero, R.A., Redondo, A., and Gnanakaran, S. (2011). Theoretical study of the remarkably diverse linkages in lignin. *J. Phys. Chem. Lett.* 2, 2660–2666.
- Parvulescu, V.I., Duraki, B., Krumeich, F., and Van Bokhoven, J.A. (2017). Lignin fragmentation onto multifunctional Fe₃O₄@Nb₂O₅@Co@Re catalysts: the role of the composition and deposition route of rhenium. *ACS Catal.* 7, 3257–3267.
- Pavia, D.L., Lampman, G.M., Kriz, G.S., and Vyvyan, J.R. (2010). *Introduction to Spectroscopy*, Fourth Edition (Brooks/Cole, Cengage Learning).
- Pham, H.N., Pagan-Torres, Y.J., Serrano-Ruiz, J.C., Wang, D., Dumesic, J.A., and Datye, A.K. (2011). Improved hydrothermal stability of niobia-supported Pd catalysts. *Appl. Catal. A Gen.* 397, 153–162.
- Pinto, M.B., Soares, A.L., Mella Orellana, A., Duarte, H.A., and De Abreu, H.A. (2017). Structural, electronic, and thermodynamic properties of the T and B phases of niobia: first-principle calculations. *J. Phys. Chem. A* 121, 2399–2409.
- Raba, A.M., Bautista-Ruiz, J., Joya, M.R., Raba, A.M., Bautista-Ruiz, J., and Joya, M.R. (2016). Synthesis and structural properties of niobium pentoxide powders: a comparative study of the growth process. *Mater. Res.* 19, 1381–1387.
- Rani, R.A., Zoofakar, A.S., O'Mullane, A.P., Austin, M.W., and Kalantar-Zadeh, K. (2014). Thin films and nanostructures of niobium pentoxide: fundamental properties, synthesis methods and applications. *J. Mater. Chem. A* 2, 15683–15703.
- Renders, T., Van den Bosch, S., Koelewijn, S.-F., Schutyser, W., and Sels, B.F. (2017). Lignin-first biomass fractionation: the advent of active stabilisation strategies. *Energy Environ. Sci.* 10, 1551–1557.
- Rinaldi, R. (2017). A tandem for lignin-first biorefinery. *Joule* 1, 427–428.
- Rinaldi, R. (2015). *Catalytic Hydrogenation for Biomass Valorization* (Royal Society of Chemistry).
- Rinaldi, R., Jastrzebski, R., Clough, M.T., Ralph, J., Kennema, M., Bruijninx, P.C.A., and Weckhuysen, B.M. (2016). Paving the way for lignin valorisation: recent advances in bioengineering, biorefining and catalysis. *Angew. Chem. Int. Ed.* 55, 8164–8215.
- Rinaldi, R., Woodward, R.T., Ferrini, P., and Rivera, H.J.E. (2019). Lignin-first biorefining of lignocellulose: The impact of process severity on the uniformity of lignin oil composition. *J. Braz. Chem. Soc.* 30, 479–491.
- Rojas, E., Guerrero-Pérez, M.O., and Bañares, M.A. (2013). Niobia-supported nanoscaled bulk-NiO catalysts for the ammoxidation of ethane into acetonitrile. *Catal. Letters* 143, 31–42.
- Samec, J.S.M. (2018). Holistic approach for converting biomass to fuels. *Chem* 4, 1199–1200.
- Schmidt, J. (2010). Electronic spectroscopy of lignins. In *Lignins and Lignans*, C. Heitner, D. Dimmel, and J. Schmidt, eds. (CRC Press), pp. 49–102.
- Schutyser, W., Renders, T., Van Den Bosch, S., Koelewijn, S.-F., Beckham, G.T., and Sels, B.F. (2018). Chemicals from lignin: an interplay of lignocellulose fractionation, depolymerisation, and upgrading. *Chem. Soc. Rev.* 47, 852–908.
- Shao, Y., Xia, Q., Dong, L., Liu, X., Han, X., Parker, S.F., Cheng, Y., Daemen, L.L., Ramirez-Cuesta, A.J., Yang, S., and Wang, Y. (2017). Selective production of arenes via direct lignin upgrading over a niobium-based catalyst. *Nat. Commun.* 8, 16104.
- Solcova, O., Uecker, D.C., Steinike, U., and Jiratova, K. (1993). Effect of the support on the reducibility of high-loaded nickel catalysts. *Appl. Catal. A Gen.* 94, 153–160.
- Sultan, Z., Graça, I., Li, Y., Lima, S., Peeva, L.G., Kim, D., Ebrahim, M.A., Rinaldi, R., and Livingston, A.G. (2019). Membrane fractionation of liquors from lignin-first biorefining. *ChemSusChem* 12, 1203–1212.
- Tanabe, K., and Okazaki, S. (1995). Various reactions catalyzed by niobium compounds and materials. *Appl. Catal. A Gen.* 133, 191–218.

Teles, C.A., de Souza, P.M., Rabelo-Neto, R.C., Griffin, M.B., Mukarakate, C., Orton, K.A., Resasco, D.E., and Noronha, F.B. (2018). Catalytic upgrading of biomass pyrolysis vapors and model compounds using niobia supported Pd catalyst. *Appl. Catal. B Environ.* 238, 38–50.

Thommes, M., Kaneko, K., Neimark, A.V., Olivier, J.P., Rodriguez-Reinoso, F., Rouquerol, J., and Sing, K.S.W. (2015). Physisorption of gases, with special reference to the evaluation of surface area and pore size distribution (IUPAC Technical Report). *Pure Appl. Chem.* 87, 1051–1069.

Valencia-Balvín, C., Pérez-Walton, S., Dalpian, G.M., and Osorio-Guillén, J.M. (2014). First-principles equation of state and phase stability of niobium pentoxide. *Comput. Mater. Sci.* 81, 133–140.

Wang, X., and Rinaldi, R. (2016). Bifunctional Ni catalysts for the one-pot conversion of organosolv lignin into cycloalkanes. *Catal. Today* 269, 48–55.

Wang, X., and Rinaldi, R. (2013). A route for lignin and bio-oil conversion: dehydroxylation of

phenols into arenes by catalytic tandem reactions. *Angew. Chem. Int. Ed.* 52, 11499–11503.

Wang, X., and Rinaldi, R. (2012). Solvent effects on the hydrogenolysis of diphenyl ether with Raney nickel and their implications for the conversion of lignin. *ChemSusChem* 5, 1455–1466.

Wojcieszak, R., Jasik, A., Monteverdi, S., Ziolk, M., and Bettahar, M.M. (2006). Nickel niobia interaction in non-classical Ni/Nb₂O₅ catalysts. *J. Mol. Catal. A Chem.* 256, 225–233.

Yin, W., Kloekhorst, A., Venderbosch, R.H., Bykova, M.V., Khromova, S.A., Yakovlev, V.A., and Heeres, H.J. (2016). Catalytic hydrotreatment of fast pyrolysis liquids in batch and continuous set-ups using a bimetallic Ni–Cu catalyst with a high metal content. *Catal. Sci. Technol.* 6, 5899–5915.

Yunker, J.M., Beste, A., and Buchanan, A.C. (2011). Computational study of bond dissociation enthalpies for substituted β-O-4 lignin model compounds. *ChemPhysChem* 12, 3556–3565.

Zhao, C., Kou, Y., Lemonidou, A.A., Li, X., and Lercher, J.A. (2010). Hydrodeoxygenation of bio-

derived phenols to hydrocarbons using RANEY® Ni and Nafion/SiO₂ catalysts. *Chem. Commun.* 46, 412–414.

Zhao, C., Kou, Y., Lemonidou, A.A., Li, X., and Lercher, J.A. (2009). Highly selective catalytic conversion of phenolic bio-oil to alkanes. *Angew. Chem. Int. Ed.* 48, 3987–3990.

Zhao, Y., Eley, C., Hu, J., Foord, J.S., Ye, L., He, H., and Tsang, S.C.E. (2012a). Shape-dependent acidity and photocatalytic activity of Nb₂O₅ nanocrystals with an active TT (001) surface. *Angew. Chem. Int. Ed.* 51, 3846–3849.

Zhao, Y., Zhou, X., Ye, L., and Edman, S.C. (2012b). Nanostructured Nb₂O₅ catalysts. *Nano Rev.* 3, 1–11.

Zhou, Y., Qiu, Z., Lü, M., Zhang, A., and Ma, Q. (2008). Preparation and spectroscopic properties of Nb₂O₅ nanorods. *J. Lumin.* 128, 1369–1372.

Ziolk, M., and Sobczak, I. (2017). The role of niobium component in heterogeneous catalysts. *Catal. Today* 285, 211–225.

ISCI, Volume 15

Supplemental Information

**Design of Nickel Supported on Water-Tolerant
Nb₂O₅ Catalysts for the Hydrotreating of Lignin
Streams Obtained from Lignin-First Biorefining**

Glauco F. Leal, Sérgio Lima, Inês Graça, Heloise Carrer, Dean H. Barrett, Erico Teixeira-Neto, Antonio Aprigio S. Curvelo, Cristiane B. Rodella, and Roberto Rinaldi

Supplemental file

Design of nickel supported on water-tolerant Nb₂O₅ catalysts for the hydrotreating of lignin streams obtained from lignin-first biorefining

Glauco F. Leal,^{a,b,c} Sérgio Lima,^a Inês Graça,^a Heloise Carrer,^c Dean H. Barrett,^{c,e} Erico Teixeira-Neto,^d Antonio Aprigio S. Curvelo,^b Cristiane B. Rodella,^c Roberto Rinaldi^{a,*}

^a Department of Chemical Engineering, Imperial College London, South Kensington Campus, London, SW7 2AZ, United Kingdom.

^b Department of Physical Chemistry, Institute of Chemistry of São Carlos, University of São Paulo, Av. Trabalhador São Carlense, 400, São Carlos, SP, 13566-590, Brazil.

^c Brazilian Synchrotron Light Laboratory (LNLS), Brazilian Center for Research in Energy and Materials (CNPEM), Campinas, SP, 13083-970, Brazil.

^d Brazilian Nanotechnology National Laboratory (LNNano), Brazilian Center for Research in Energy and Materials (CNPEM), Campinas, SP, 13083-970, Brazil.

^e School of Chemistry, University of the Witwatersrand, Johannesburg, South Africa

*Corresponding author: R. Rinaldi, e-mail: rrinaldi@ic.ac.uk.

Transparent Methods

Catalysts synthesis

Niobia synthesis by hydrothermal method. TT-Nb₂O₅ nanorods were prepared by dissolving ammonium niobium oxalate (5.22 g; 99.9%, CBMM) in deionized water (65 mL) and H₂O₂ (15 mL, 30%, Synth) in a molar ratio H₂O₂:Nb of 10, forming a yellowish solution.(Leal et al., 2019) This solution was then transferred to a 150 mL stainless steel reactor equipped with a PTFE liner, for a hydrothermal treatment at 175°C for 15 h. The hydrothermal treatment produced a white precipitate of Nb₂O₅. The solid was separated by filtration and washed with deionized water several times. Next, the solid was dried overnight in an oven at 60°C. To obtain the final support (TT-Nb₂O₅), the material was calcined in a muffle at 380°C for 2 h.

Preparation of Ni/Nb₂O₅ catalysts. Ni was deposited on the Nb₂O₅ material by employing a deposition-precipitation ammonia evaporation method.(Leal et al., 2019) Typically, Nb₂O₅ (1.0 g), (NH₄)₂CO₃ (2.0 g, Sigma-Aldrich) and NiCO₃·2Ni(OH)₂·xH₂O (in quantities to provide a 5, 10, 15, and 25 wt% Ni, 99.9%, Sigma-Aldrich) were dispersed in deionized water (20 mL). To the mixture, an aqueous NH₄OH solution (20 mL, 26-30%, Sigma-Aldrich) was added. The suspension was then kept under magnetic stirring at 90°C for 3 h, under N₂ flow. The solid was centrifuged and washed with deionized water several times until the filtrate showed a neutral pH value. Next, the solid was dried at 110°C overnight in an oven. The dried Ni/Nb₂O₅ catalyst precursor was reduced in a tubular oven under H₂ flow. The sample was heated up to 320°C with a heating ramp of 5°C min⁻¹, and kept at 320°C for 1.5 h under H₂ atmosphere. The reduced Ni/Nb₂O₅ catalyst was cooled down to room temperature

under Ar flow and stored under Ar atmosphere in a glove box. The catalysts were referred to as %Ni/Nb₂O₅, where %Ni represents the nominal Ni loading on Nb₂O₅.

Catalyst characterizations

Ni loading. Ni loading on Nb₂O₅ (Table 1) was determined by inductively coupled plasma – mass spectroscopy (ICP-MS) analysis on an Agilent Technologies 7900 ICP-MS system. For the analysis, a catalyst sample (5 mg) was suspended in HNO₃ (10 mL, >68%, Fisher Chemical) and digested under microwave irradiation at 200°C for 15 min by using a CEM MARS6 microwave oven. After digestion, an aliquot of the solution (0.1 mL) was diluted 10-times in deionized water (9.9 mL). The solution was then analyzed on the ICP-MS. For each sample, the determination of Ni and Nb was carried out in triplicate.

Powder X-Ray diffraction. X-Ray diffraction (XRD) measurements were performed on the XPD beamline at the Brazilian Synchrotron Light Laboratory (LNLS), operating at an energy of 8keV ($\lambda = 1.5498 \text{ \AA}$). XRD patterns were collected in a 2θ angular range from 15 to 90° with a Mythen – 1K linear detector (Dectris) installed at 1 m from the sample. Crystalline phases were identified by comparison with JCPDS files. Ni crystallite size was estimated by using the Scherrer equation, with the full-width at half-maximum (FWHM) of the peaks being determined by fitting the data in a pseudo-Voigt function.

Scanning transmission electron microscopy. Scanning transmission electron microscopy (STEM) was performed in the LNNano facilities, CNPEM, Brazil. Acquisition of High-Angle Annular Dark-Field (HAADF) images was performed in an

FEI Titan Themis aberration-corrected scanning electron microscope operating at 300 kV. The samples were prepared by applying the catalyst powders directly over TEM standard specimen holder.

Textural properties. The surface area was determined by adsorption-desorption isotherms of N₂ at -196°C in an Autosorb 1C (Quantachrome). The samples were pretreated at 120°C overnight under vacuum. The specific surface area was determined by the BET method.

Temperature-programmed reduction of Ni/Nb₂O₅. The reduction of the Ni/Nb₂O₅ catalyst precursor was analyzed by H₂ temperature-programmed reduction (TPR). The precursor samples (50 mg) were pre-treated at 150°C for 1 h under He flow (50 mL min⁻¹). TPR analysis was then performed from room temperature to 1000°C at a heating rate of 10°C min⁻¹ under 5% H₂/He flow (50 mL min⁻¹). H₂ was monitored by a mass spectrometer OmniStar™ GSD 320 O1 (Pfeiffer Vacuum).

ATR-FTIR pyridine adsorbed on Ni/Nb₂O₅. The acidic properties of niobium oxide support were evaluated by attenuated total reflection Fourier Transform infrared spectroscopy (ATR-FTIR) of adsorbed pyridine (Py). FTIR spectra were collected on an FTIR spectrometer from Perkin Elmer (Spectrum Two) in the range from 400 to 4000 cm⁻¹ at a resolution of 0.5 cm⁻¹. For signal accumulation, 32 scans were collected. Initially, the samples in powder form were dried at 150°C for 1h, under N₂ flow, in a three-neck rounded bottle flask (50 mL) equipped with a heating mantle. N₂ carried pyridine (Py) vapor was introduced into the flask for the adsorption of pyridine on Nb₂O₅ and reduced Ni/Nb₂O₅ samples. Next, the sample was exposed to Py vapor at 150°C for 1 h. Then, the flask was purged with N₂ at 120°C, for 30 min, to remove

physisorbed Py. After cooling to room temperature, the sample was transferred to an eppendorf and the FTIR spectra were collected with the ATR probe. The spectrum of adsorbed Py was obtained by subtracting the spectrum of the sample with chemisorbed Py from that of the treated sample without pyridine.

Quantification of Brønsted and Lewis acid sites by FTIR of adsorbed pyridine on Nb₂O₅. The acidic properties of the niobium oxide were evaluated by FTIR of the samples adsorbed with pyridine (Py). The FTIR spectra were collected using a Nicolet FT-IR-6700 spectrometer in the range from 4000 to 1000 cm⁻¹ with a resolution of 2 cm⁻¹ and 128 scans for signal accumulation. The samples were prepared as a thin pellet through pressing sample powder. The sample pellet was transferred into a homemade IR cell equipped with CaF windows. First, the sample was dehydrated at 120 °C under dynamic vacuum (2·10⁻⁵ mbar) for 22 h. After cooled down to room temperature, the sample spectrum was obtained. Then, the sample was exposed to Py vapor until the equilibrium with vapor pressure and cooked at 150 °C for 20 h. Next, the system was cooled down to room temperature and kept under dynamic vacuum (2·10⁻⁵ mbar) for 30 min to remove the physisorbed Py and collected the FTIR spectrum. The quantification of acid sites was done using the Lambert-Beer equation ($A_i = \epsilon_i \cdot c \cdot d$) using the integrated absorbance (A_i) and the Integrated Molar Absorption Coefficient (ϵ_i). (Barzetti et al., 1996) The bands in 1444 cm⁻¹ ($\epsilon_i = 2.22 \text{ cm } \mu\text{mol}^{-1}$) and 1540 cm⁻¹ ($\epsilon_i = 1.67 \text{ cm } \mu\text{mol}^{-1}$) (Emeis, 1993) were used to quantify Lewis Acid Sites (LAS) and Brønsted Acid Sites (BAS), respectively.

Catalyst tests

Hydrodeoxygenation of diphenyl ether. The experiments were carried out in a stainless steel batch reactor (250 mL) using a catalyst (0.500 g) suspended in a 0.19 mol L⁻¹ solution of diphenyl ether (13.5 mmol, Sigma-Aldrich, 99%), containing *n*-dibutyl ether (0.052 mol L⁻¹, 3.64 mmol, Acros Organics, > 99%, internal standard for GC analysis) and methylcyclohexane (70 mL, Acros Organics, 99%, solvent) under mechanical stirring at 400 rpm. All processes involving the fresh catalyst manipulation and reactor loading were carried out in a glove box under Ar atmosphere. The reactor was purged with H₂ and loaded with 4 MPa at 25°C. The experiments were performed at 160 or 200°C for 180 min. Reaction mixture aliquots at 0, 15, 30, 60, 90, 120 and 180 min were collected. Recycling experiments were performed at 200°C, under similar operating conditions. Five reaction cycles of 240 min were carried out. After each cycle, the catalysts were separated from the reaction mixture by vacuum filtration, washed with methylcyclohexane and dried in a vacuum oven at 40°C overnight.

The reaction products were analyzed in a gas chromatograph (Shimadzu QP2010 Plus) equipped with a Rxi-1ms capillary column (30 m, 0.25 mm ID, df 0.25 mm). The following temperature program was used: an isothermal step for 5 min at 40°C, increase in temperature at 5.2°C min⁻¹ up to 300 °C and finally an isothermal step for 5 min at 300°C. The quantification was performed using a multi-point internal standard method, through calibration curves based on the response of the flame ionization detector (FID) for each component relative to the internal standard response.

Catalytic Upstream Biorefining to produce the lignin oil stream. The catalytic upstream biorefining (CUB) process was used to deconstruct poplar wood, rendering lignin oil and a holocellulosic pulp.(Ferrini and Rinaldi, 2014) Poplar wood pellets (704 g) and Raney Ni (331 g, wet) were suspended in an aqueous solution of 2-PrOH (4140 mL, 70%, v/v) and placed in a 2 gallon (ca. 9 L) stainless steel batch reactor (Parr Instruments & Co, model number: 4552). The suspension was stirred (75 rpm) for 30 min at room temperature. Then, the reactor was heated to 200°C in 1h under mechanical stirring (700 rpm). The reaction proceeded under autogenic pressure for 3 h. In sequence, the mixture was allowed to cool down to room temperature. The liquor was separated from the solids (Raney Ni in conjunction with the holocellulosic pulp) by filtration through a glass fiber filter (GF6, Ø 90 mm, Whatman). The solids were re-suspended in a 2-PrOH/H₂O mixture in a PE beaker under mechanical stirring. To separate Raney Ni from the suspension, a strong neodymium magnet was externally placed on the bottom of the beaker. The suspension was mechanically stirred, resulting in the detachment of catalyst particles from the pulp, which were magnetically decanted. Keeping the magnet placed on the bottom of the beaker, the catalyst was separated from the pulp suspension by pouring the suspension into a Buchner funnel. The catalyst was recovered by removing the magnet. The liquor was isolated from the pulp by filtration under reduced pressure. The catalyst separation procedure was repeated three times to remove the catalyst content from the pulp fibers. The liquor and the filtrates (obtained from the catalyst separation procedure) were combined. Finally, the lignin oil stream was isolated by removing the solvent from the liquor and filtrates by using a rotoevaporator at 45°C under vacuum.

Hydrodeoxygenation of lignin oil. The produced lignin oil (2.000 g), *n*-pentane (70 mL), 15%Ni/Nb₂O₅ (0.400 g) were placed in a 600 mL stainless Parr batch reactor. All steps involving the fresh catalyst manipulation and reactor loading were performed inside a glove box under Ar atmosphere. The reactor was then pressurized to 7 MPa with H₂ (measured at room temperature). The pressure vessel was then heated up to 300°C and the reaction proceed for 16 h under mechanical stirring (400 rpm). In sequence, the mixture was allowed to cool down to room temperature. Then, the liquid fraction was separated from the residual solid, composed of catalyst and lignin residues, by filtration. Finally, to isolate the liquid products, the solvent of the collected liquid fraction was evaporated at 25°C by using a centrifugal evaporator (Centrifan™ PE, KDScientific). To recover the spent catalyst for recycling, the mixture of catalyst and lignin residue was washed with methanol. This procedure could dissolve about 10% of the polymeric lignin residue. The suspension was filtered. After solvent removal, the lignin residue soluble in methanol was set apart for characterization. In turn, the washed solid residue (catalyst containing lignin residue insoluble in methanol) was dried at 40 °C overnight under vacuum and weighed to determine the net conversion of lignin. The net conversion of the lignin oil was calculated by Eq. S1:

$$Net\ conversion = \left(1 - \frac{mass_{washed\ solid\ residue} - initial\ mass_{catalyst}}{mass_{lignin\ oil}} \right) \times 100 \quad (S1)$$

The liquid products and the solid residue soluble in methanol were analyzed by CHNS/O elemental analysis, GPC and GC-FID/MS.

Analysis of lignin oil products

GC-FID/MS analysis. An aliquot of each sample (20.0 mg) and the external standard (di-*n*-butyl ether, the internal standard for GC analysis, 3.0 mg) were dissolved in MeOH (1 mL). The sample was filtered (membrane filter 0.45 µm). The sample solutions were analyzed by GC-MS 2010 Plus (Shimadzu) equipped with a capillary column DB-1MS (30 m, 0.25 mm ID, df 0.25 µm). The following temperature program was used: an isothermal step for 5 min at 40 °C, increase in temperature at 5.2°C min⁻¹ up to 300°C and, finally, an additional isothermal step for 5 min at 300°C. Quantification of selected components was performed by using the FID response. The response factor of the products was determined from calibration curves (for cyclohexane, cyclohexanol, 4-ethylcyclohexanol, phenol, 4-ethylphenol, 2-methoxy-4-ethylphenol, 2-methoxy-4-propylphenol, 2,6-dimethoxyphenol, 2,6-dimethoxy-4-methylphenol, 4-(3-hydroxypropyl)-2-methoxyphenol, 4-allyl-2,6-dimethoxyphenol) or by using the Effective Carbon Number method (ECN, for 2,6-dimethoxy-4-ethylphenol, 2,6-dimethoxy-4-propylphenol) relative to 2,6-dimethoxy-4-methylphenol. (Scanlon and Willis, 1985)

Gel permeation chromatography analysis. To analyze the apparent molecular weight distribution in lignin products, the products (20 mg) were dissolved in a solution of anhydrous dimethylformamide (DMF) containing 0.1 wt% LiBr (1 mL) and filtered (membrane filter 0.45 µm) prior to injection. The GPC analyses were performed at 60°C with a Shimadzu HPLC Prominence system equipped with three columns (Polargel-M guard 50x4.6mm, Polargel-M 300x7.5mm, Polargel-L 300x7.5mm, Agilent), and by using DMF + LiBr 0.1 wt% as the eluent (1.0 mL min⁻¹). For detection,

a Shimadzu SPD-M20A diode-array detector (PDA) was used. All responses were normalized by the sample weight. The system was calibrated with polystyrene standards (200 to 60 000 Da, Aldrich).

CHN/O elemental analysis. CHN/O elemental analyses of the products were carried out in an Elementar VarioMI-CRO Cube analyzer, by using 1-2 mg of the sample. Each sample was analyzed in triplicate, and the average value was taken. The oxygen content in the samples was estimated by subtraction ($\%O = 100 - \%C - \%H - \%N$).

Total organic carbon. Total organic carbon content in the aqueous product was determined in a Sievers InnovOx Laboratory TOC analyzer provided by GE Instruments, by diluting 50 μ L of the sample with deionized water to obtain a total volume of 20 mL.

Nitrogen adsorption-desorption measurements

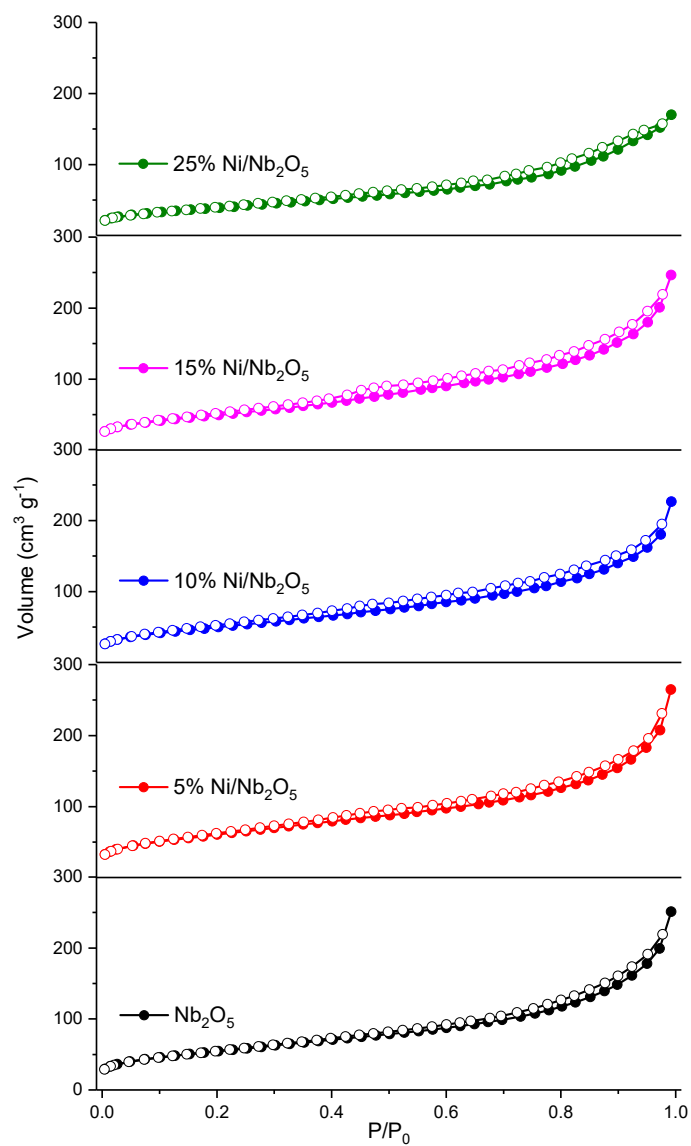


Figure S1. N₂ adsorption-desorption isotherms of the support and Ni/Nb₂O₅ catalysts, related to Table 1.

Table S1. Temperatures of reduction of NiO and Nb₂O₅ species in Nb₂O₅ and Ni/Nb₂O₅ materials, related to Figure 3.

Sample	Reduction temperature (°C)	
	NiO	Nb ₂ O ₅
Nb ₂ O ₅	----	870
5%Ni/Nb ₂ O ₅	339	847
10%Ni/Nb ₂ O ₅	334	847
15%Ni/Nb ₂ O ₅	346	834
25%Ni/Nb ₂ O ₅	338	816

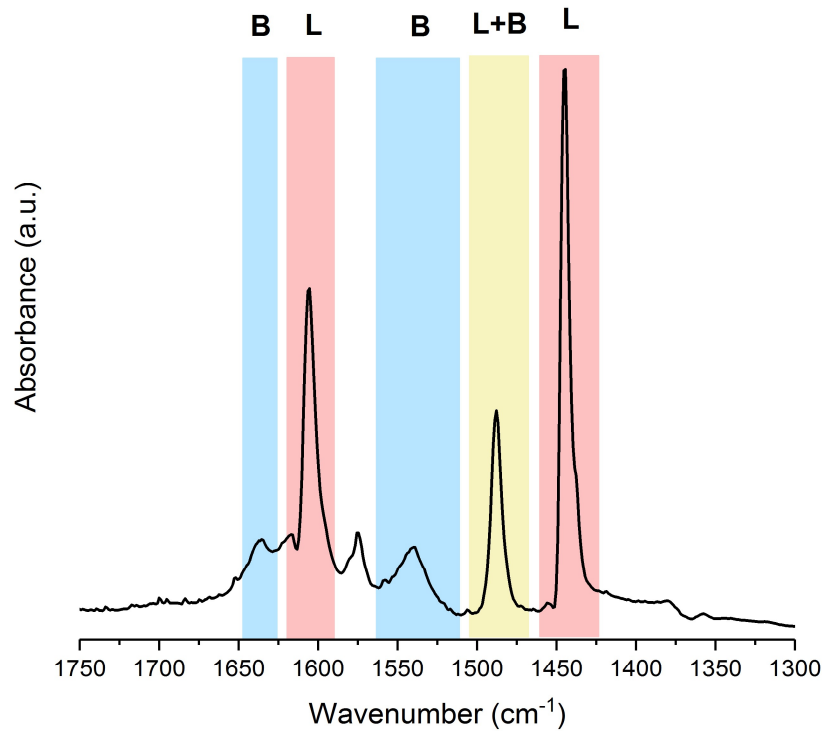


Figure S2. FTIR absorption spectrum of pyridine adsorbed on Nb₂O₅, relate to Figure 4.

Table S2. Amount of Brønsted and Lewis sites in the niobia, relate to Figure S2.

	Area 1444 cm ⁻¹	Lewis acidity (μmol g ⁻¹)	Area 1540 cm ⁻¹	Brønsted acidity (μmol g ⁻¹)
Nb ₂ O ₅	0.466	210	0.239	143

Table S3. Conversion and products distribution of the diphenyl ether hydrogenation reaction in the absence of a catalyst and using only the niobium oxide at 160 °C and 4 MPa H₂ pressure, relate to Table 3.

c1ccc(Oc2ccccc2)cc1 (1) → c1ccc(Oc2ccccc2)cc1 (2) + C1CCC(CC1)OC2CCCCC2 (3) + Oc1ccc(cc1)c2ccccc2 (4) + c1ccccc1 (5) + Oc1ccccc1 (6) + C1CCC(CC1) (7)

Catalyst	Conversion (%)	Time (min)	Yield (%)					
			2	3	4	5	6	7
Blank reaction	8	180	1.5	0.3	0.2	0.6	2.8	2.5
Nb(HT)	15	180	4.4	1.1	0.3	1.1	2.3	4

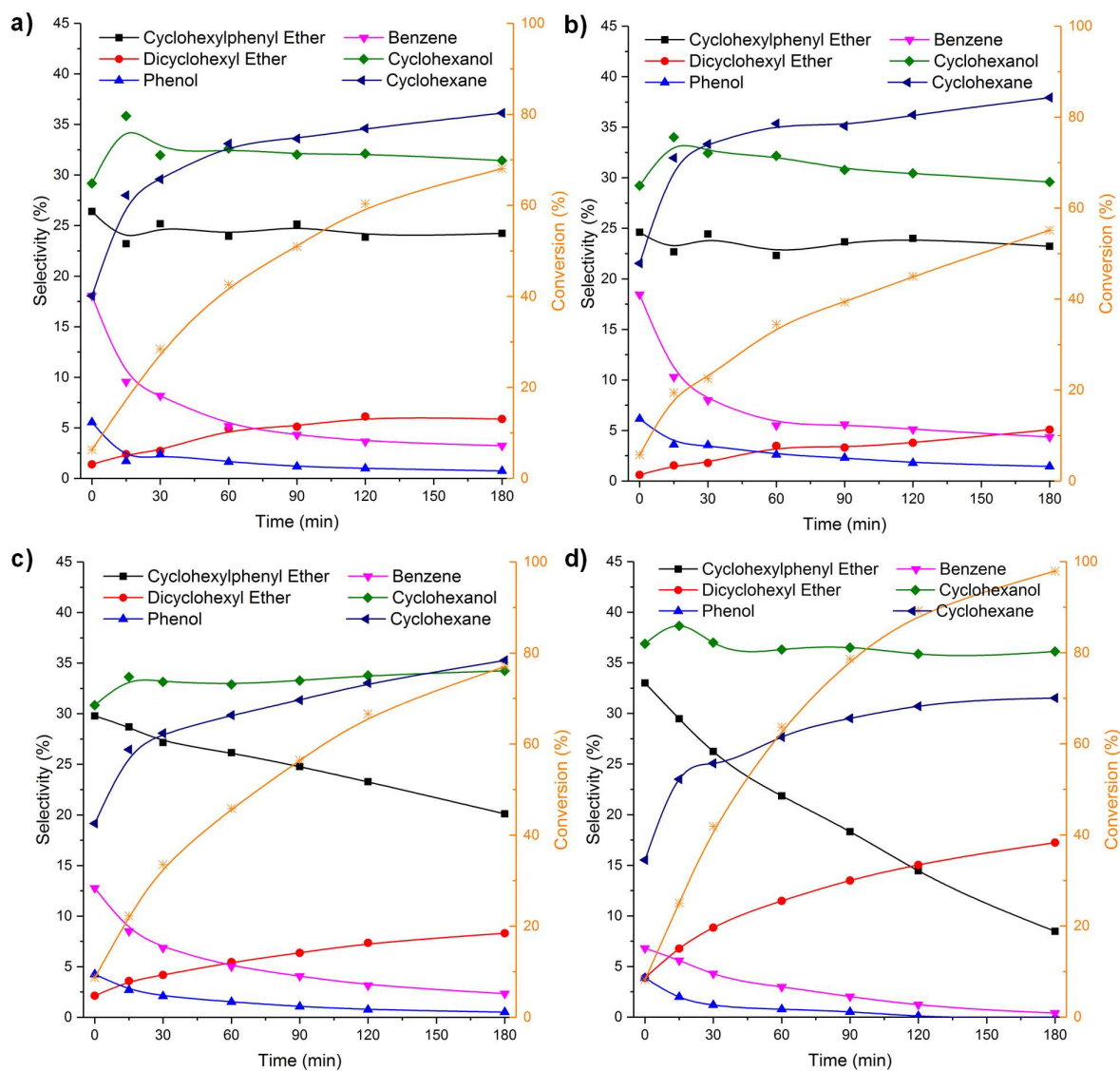
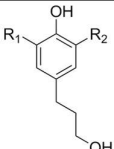
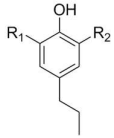
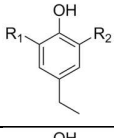
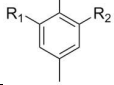
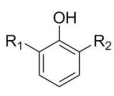
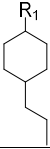
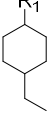
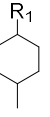
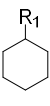


Figure S3. Products selectivity in diphenyl ether hydrodeoxygenation employing as a catalyst: a) 5%Ni/Nb₂O₅; b) 10%Ni/Nb₂O₅; c) 15%Ni/Nb₂O₅ and d) 25%Ni/Nb₂O₅. Conversion of diphenyl ether shown by orange-coded lines, relate to Table 3 and Figure 6.

Table S4. Weight content of selected components in the lignin oil, liquid organic products of the hydrotreating of lignin oil over 15%Ni/Nb₂O₅, and control experiment (no added catalyst) as determined by GC-FID/MS analysis, relate to Figure 13.

Selected component	Content (wt%)					
	Lignin Bio-oil	1 st Run	2 nd Run	3 rd Run	Control experiment	
	R ₁ = H; R ₂ = OCH ₃	9.7	0	0	0	1.5
	R ₁ = R ₂ = OCH ₃	9.3	0	0	0	0
	R ₁ = R ₂ = H	0.2	0	1.5	1.2	0.3
	R ₁ = H; R ₂ = OCH ₃	0.6	0	3.3	2.9	9.4
	R ₁ = R ₂ = OCH ₃	1.6	0	1.2	1.4	0
	R ₁ = R ₂ = H	0.5	0	2.9	2.2	1.2
	R ₁ = H; R ₂ = OCH ₃	0.6	0	6.3	7.0	8.9
	R ₁ = R ₂ = OCH ₃	1.3	0	0	0	0
	R ₁ = H; R ₂ = OCH ₃	0	0	0.8	0.8	0.7
	R ₁ = R ₂ = H	2.8	0	0.6	0.6	6.6
	R ₁ = H; R ₂ = OCH ₃	0	0	0.9	1.4	4.5
	R ₁ = R ₂ = OCH ₃	0.2	0	0.9	1.4	0.3
Aliphatic double ring products		0	22	3.8	2.3	0
	R ₁ = H	0	16	1.0	1.2	0
	R ₁ = OH	0.6	1.6	11.5	8.9	2.9
	R ₁ = H	0	4.3	0	0	0
	R ₁ = OH	0.7	0	11	13	2.7
	R ₁ = H	0	0.3	0.07	0.1	0
	R ₁ = OH	0	0	1.0	1.2	0
	R ₁ = H	0	0.2	3.0	0.9	1.3
	R ₁ = OH	0	0	7.1	12	1.0
	R ₁ = C ₅ , C ₇	0	4.6	0	0	0
Sum of selected components		28	49	57	58	41

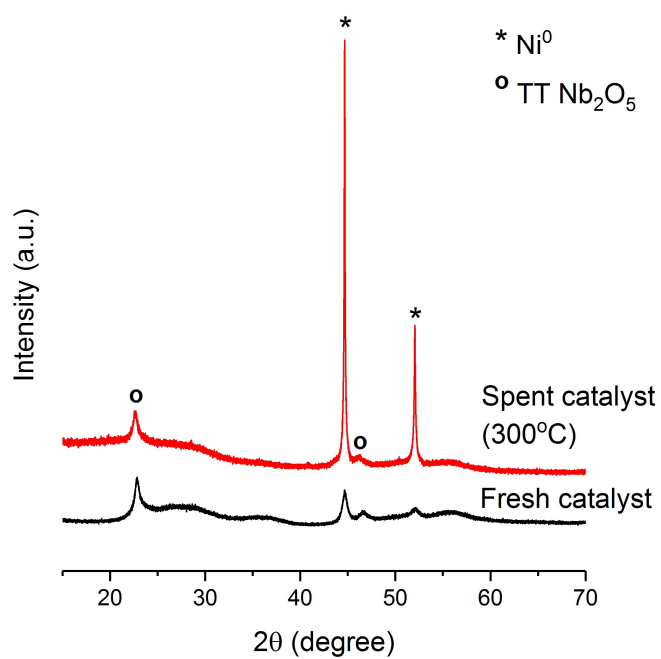


Figure S4. XRD patterns of the 15% Ni/Nb₂O₅ catalyst before and after catalyst recycling at 300 °C (third run), relate to Figure 14.

References

- Barzetti, T., Selli, E., Moscotti, D., Forni, L., 1996. Pyridine and ammonia as probes for FTIR analysis of solid acid catalysts. *J. Chem. Soc. Faraday Trans.* 92, 1401.
- Emeis, C.A., 1993. Determination of integrated molar extinction coefficients for infrared absorption bands of pyridine adsorbed on solid acid catalysts. *J. Catal.* 141, 347–354.
- Ferrini, P., Rinaldi, R., 2014. Catalytic biorefining of plant biomass to non-pyrolytic lignin bio-oil and carbohydrates through hydrogen transfer reactions. *Angew. Chem. Int. Ed.* 53, 8634–8639.
- Leal, G.F., Barrett, D.H., Carrer, H., Figueroa, S.J.A., Teixeira-Neto, E., Curvelo, A.A.S., Rodella, C.B., 2019. Morphological, Structural, and Chemical Properties of Thermally Stable Ni-Nb₂O₅ for Catalytic Applications. *J. Phys. Chem. C* 123, 3130–3143.
- Scanlon, J.T., Willis, D.E., 1985. Calculation of flame ionization detector relative response factors using the effective carbon number concept. *J. Chromatogr. Sci.* 23, 333–340.
- Wang, X., Rinaldi, R., 2016. Bifunctional Ni catalysts for the one-pot conversion of Organosolv lignin into cycloalkanes. *Catal. Today* 269, 48–55.